Reactive-diffusive phenomena in two-dimensional, anisotropic media

J.I. Ramos
Universidad de Málaga, Málaga, Spain

Received August 2002
Revised May 2003
Accepted June 2003

Keywords *Physical properties of materials, Approximation theory*

Abstract *Non-linear reaction-diffusion processes with cross-diffusion in two-dimensional, anisotropic media are analyzed by means of an implicit, iterative, time-linearized approximate factorization technique as functions of the anisotropy of the heat and species diffusivity tensors, the Soret and Dufour cross-diffusion effects, and five types of boundary conditions. It is shown that anisotropy and cross-diffusion deform the reaction front and affect the front velocity, and the magnitude of these effects increases as the magnitude of the off-diagonal components of the heat and species diffusivity tensors is increased. It is also shown that the five types of boundary conditions employed in this study produce similar results except when there is either strong anisotropy in the species or heat diffusivity tensors and there are no Soret and Dufour effects, or the species and heat diffusivity tensors are isotropic, but the anisotropy of the Soret and Dufour effects is important. If the species and heat diffusivity tensors are isotropic, the effects of either the Soret or the Dufour cross-diffusion effects are small for the cases considered in this study. The time required to achieve steady state depends on the anisotropy of the heat and diffusivity tensors, the cross-diffusion effects, and the boundary conditions.*

1. Introduction

Many materials are non-homogeneous and anisotropic, and the dependence of their thermal conductivity on the space coordinates and direction must be considered. Examples of anisotropic materials include wood, sedimentary rocks, laminated metal sheets, fibre reinforced structures, porous media and composites, to name a few.

The appearance of mixed second-order derivatives and the boundary conditions have placed great challenges in analytical studies of even linear anisotropic heat conduction problems (Hsieh and Ma, 2002), and researchers have employed a variety of approximate numerical techniques including Monte Carlo methods for steady state situations (Kowsary and Arabi, 1999), lumped-differential formulations for the study of steady anisotropic heat transfer in composite materials (Traiano *et al.*, 1997), finite element methods for the curing of thermosetting matrix composites (Yi *et al.*, 1997), and boundary element formulations for steady anisotropic heat conduction problems in

This research was partially financed by Project BFM2001-1902 from the Ministerio de Educación y Ciencia of Spain and fondos FEDER. The author is grateful to the referees for their comments that have contributed to a better presentation of the results.

International Journal of Numerical Methods for Heat & Fluid Flow
Vol. 13 No. 8, 2003
pp. 997-1030

0961-5539
DOI 10.1108/09615530310501939

two-dimensional domains (Mera *et al.*, 2001). All of these studies have considered linear problems without source terms, except that of Yi *et al.* (1997) that accounted for internal heat generation by exothermic chemical reactions in their simulations of the curing of polymer matrix composites; these authors assumed that the degree of curing is governed by the first-order ordinary differential equations in the time variable which depend non-linearly on the temperature which, in turn, is governed by a partial differential equation with an isotropic thermal conductivity tensor.

In this paper, we consider non-linear reaction-diffusion phenomena in two-dimensional anisotropic media such as those occurring in combustion of solid materials, reactive flows in porous media, catalysts, curing of composite materials, etc., subject to different boundary conditions, by accounting for the anisotropic character of both the species and heat diffusion. In addition, the formulation presented in the paper accounts for anisotropic cross-diffusion effects, i.e. the effects of heat conduction on the diffusion of chemical species and the effects of species diffusion on heat conduction, which have been ignored in earlier studies of flows in porous media, curing of materials and laser-induced thermal damage of laminated composites. These effects are called the (thermodiffusion) Soret and Dufour ones and may play an important role in transport phenomena in reactive and/or diffusive media (Skarda *et al.*, 1998; Williams, 1985) and porous media with thermal and solutal convection (Benano-Melly *et al.*, 2001) to name, but a few. The formulation presented in this paper is given in terms of dimensionless variables and can also be applied to study a variety of two-dimensional reactive-diffusive systems with anisotropic heat conductivity and diffusivity tensors such as those mentioned above.

As stated earlier, even two-dimensional anisotropic heat conduction problems are not easily amenable to analytical techniques due to the appearance of mixed second-order derivative terms. In this paper, implicit, iterative, time-linearization methods based on the discretization of the time variable and the linearization of the resulting elliptic partial differential equations with respect to the previous time level are employed. These (two-dimensional) linear elliptic equations are then factorized in terms of one-dimensional operators in each spatial direction taking into consideration the mixed second-order derivative terms and neglecting the second-order factorization errors.

Approximate factorization methods for non-linear problems including the Euler and Navier-Stokes equations were developed by Beam and Warming (1978) and Briley and McDonald (1980). The approximate factorization of the two-dimensional compressible Navier-Stokes equations cannot be performed exactly due to the appearance of mixed second-order derivatives in the linear momentum equations; these terms are analogous to those that appear in the anisotropic reactive-diffusive media considered in this paper and have, in the

past, been evaluated explicitly either at the previous time level with the consequent loss of accuracy of the resulting implicit time-linearized method or using two previous time levels which maintain the second-order accuracy of second-order implicit time-linearized techniques at the expense of introducing additional time levels (Beam and Warming, 1978; Briley and McDonald, 2001; Steinthorsson *et al.*, 1991).

In this paper, an approximate factorization method is employed and the mixed second-order derivative terms and the implementation of the boundary conditions are treated iteratively by means of the iterative predictor-corrector strategy proposed by Ramos (1999) in his study of two-dimensional reaction-diffusion equations in the isotropic media. Iterative approximate factorization techniques have been recently reviewed by Briley and McDonald (2001) and MacCormack (2001) who point out that non-iterative approximate factorization techniques should be used whenever one is interested in the (final) steady-state solution, whereas iterative ones should be employed whenever one is interested in accurate transient solutions.

The paper has been organized as follows. In Section 2, the non-dimensional time-dependent equations governing the reactive-diffusive phenomena in two-dimensional anisotropic media are presented. Section 3 contains a study of the convergence of the iterative predictor-corrector strategy and an analysis of the linear stability of the numerical method employed in this paper. The iterative approximate factorization technique has been employed to deal with the mixed second-order derivative terms and the boundary conditions, and originates from the time discretization and both the linearization with respect to the previous time level and the factorization of the resulting elliptic equations. Some sample results illustrating the transient phenomena in the two-dimensional, anisotropic, reactive-diffusive media are presented in Section 4, as functions of the anisotropy of the heat conductivity and species diffusion tensors as well as the Soret and Dufour or cross-diffusion effects, and five different types of boundary conditions. Section 5 provides a summary of the main conclusions.

2. Formulation

Consider the following system of two, non-linearly coupled, reaction-diffusion (partial differential) equations

$$\frac{\partial u}{\partial t} = \nabla \cdot (\mathbf{k} \nabla u) + \nabla \cdot (\mathbf{d} \nabla v) + S_u(u, v), \tag{1}$$

$$\frac{\partial v}{\partial t} = \nabla \cdot (\mathbf{K} \nabla u) + \nabla \cdot (\mathbf{D} \nabla v) + S_v(u, v), \tag{2}$$

where t is the time variable, u and v are the dependent variables, **k**, **d**, **K** and **D** are the diffusivity tensors, S_u and S_v are the non-linear source terms, and ∇ is the gradient operator in the two-dimensional Cartesian coordinates x and y.

The diffusivity tensors considered in this paper may not be diagonal; therefore, equations (1) and (2) contain mixed second-order derivative terms. Equations (1) and (2) can also be written as

$$\frac{\partial \mathbf{U}}{\partial t} = \alpha \frac{\partial^2 \mathbf{U}}{\partial x^2} + \beta \frac{\partial^2 \mathbf{U}}{\partial x \partial y} + \gamma \frac{\partial^2 \mathbf{U}}{\partial y^2} + \mathbf{S}(\mathbf{U}), \tag{3}$$

where $\mathbf{U} = (u, v)^{\mathrm{T}}$, $\mathbf{S} = (S_u, S_v)^{\mathrm{T}}$, the superscript T denotes transpose, and α, β and γ are the second-order rank tensors. The components of α are $\alpha_{11} = k_{11}$, $\alpha_{12} = d_{11}$, $\alpha_{21} = K_{11}$ and $\alpha_{22} = D_{11}$, those of β are $\beta_{11} = k_{12} + k_{21}$, $\beta_{12} = d_{12} + d_{21}$, $\beta_{21} = K_{12} + K_{21}$, and $\beta_{22} = D_{12} + D_{21}$, and those of γ are $\gamma_{11} = k_{22}$, $\gamma_{12} = d_{22}$, $\gamma_{21} = K_{22}$, and $\gamma_{22} = D_{22}$. Hereon, we shall refer to u and v as the species mass fraction and (non-dimensional) temperature, respectively; **k** and **D** as the species and heat diffusivity tensors, respectively; and, the second term on the right-hand side of equation (1) and the first term on the right-hand side of equation (2) as either the effects of heat and species diffusion on species and heat diffusion, respectively, or the Soret and Dufour cross-diffusion effects, respectively, by analogy with the terminology employed in transport phenomena and, especially, in combustion (Williams, 1985).

Equations (1) and (2) govern a variety of physical problems such as, for example, non-linear reaction-diffusion processes in the anisotropic media, the curing of thermosetting matrix composites, anisotropic heat and mass transfer, combustion of solid materials, etc.

In this paper, we consider the solution of equations (1) and (2) in $D = [-L_x/2 < x < L_x/2, -L_y/2 < y < L_y/2]$ and $t > 0$, where $L_x = L_y = 20$, initial conditions $\mathbf{U}(0, x, y) = (1, v_i)^{\mathrm{T}}$ where $v_i = \exp(-(x^2 + y^2))$ which correspond to a local increase of the temperature, for $\mathbf{S} = (-u^2 v, u^2 v - 0.5v)^{\mathrm{T}}$, different diffusivity tensors, and the following types of (Neumann) boundary conditions.

Boundary conditions of type 1:

$$\frac{\partial u}{\partial n} = \frac{\partial v}{\partial n} = 0, \tag{4}$$

on all the boundaries, where n denotes the external normal to the boundary.

Boundary conditions of type 2:

$$\frac{\partial u}{\partial x} = \frac{\partial v}{\partial x} = 0, \quad \text{at} \quad x = \pm L_x, \tag{5}$$

$$k_{21}\frac{\partial u}{\partial x}+k_{22}\frac{\partial u}{\partial y}=0,\quad \text{at}\quad y=\pm L_y, \tag{6}$$

$$D_{21}\frac{\partial v}{\partial x}+D_{22}\frac{\partial v}{\partial y}=0,\quad \text{at}\quad y=\pm L_y. \tag{7}$$

Boundary conditions of type 3:

$$\frac{\partial u}{\partial x}=\frac{\partial v}{\partial x}=0,\quad \text{at}\quad x=\pm L_x, \tag{8}$$

$$k_{21}\frac{\partial u}{\partial x}+k_{22}\frac{\partial u}{\partial y}+d_{21}\frac{\partial v}{\partial x}+d_{22}\frac{\partial v}{\partial y}=0,\quad \text{at}\quad y=\pm L_y, \tag{9}$$

$$K_{21}\frac{\partial u}{\partial x}+K_{22}\frac{\partial u}{\partial y}+D_{21}\frac{\partial v}{\partial x}+D_{22}\frac{\partial v}{\partial y}=0,\quad \text{at}\quad y=\pm L_y. \tag{10}$$

Boundary conditions of type 4:

$$k_{11}\frac{\partial u}{\partial x}+k_{12}\frac{\partial u}{\partial y}+d_{12}\frac{\partial v}{\partial y}=0,\quad \text{at}\quad x=\pm L_x, \tag{11}$$

$$K_{12}\frac{\partial u}{\partial y}+D_{11}\frac{\partial v}{\partial x}+D_{12}\frac{\partial v}{\partial y}=0,\quad \text{at}\quad x=\pm L_x. \tag{12}$$

$$k_{21}\frac{\partial u}{\partial x}+k_{22}\frac{\partial u}{\partial y}+d_{21}\frac{\partial v}{\partial x}+d_{22}\frac{\partial v}{\partial y}=0,\quad \text{at}\quad y=\pm L_y, \tag{13}$$

$$K_{21}\frac{\partial u}{\partial x}+K_{22}\frac{\partial u}{\partial y}+D_{21}\frac{\partial v}{\partial x}+D_{22}\frac{\partial v}{\partial y}=0,\quad \text{at}\quad y=\pm L_y. \tag{14}$$

Boundary conditions of type 5:

$$k_{11}\frac{\partial u}{\partial x}+k_{12}\frac{\partial u}{\partial y}+d_{11}\frac{\partial v}{\partial x}+d_{12}\frac{\partial v}{\partial y}=0,\quad \text{at}\quad x=\pm L_x, \tag{15}$$

$$K_{11}\frac{\partial u}{\partial x}+K_{12}\frac{\partial u}{\partial y}+D_{11}\frac{\partial v}{\partial x}+D_{12}\frac{\partial v}{\partial y}=0,\quad \text{at}\quad x=\pm L_x. \tag{16}$$

$$k_{21}\frac{\partial u}{\partial x}+k_{22}\frac{\partial u}{\partial y}+d_{21}\frac{\partial v}{\partial x}+d_{22}\frac{\partial v}{\partial y}=0,\quad \text{at}\quad y=\pm L_y, \tag{17}$$

$$K_{21}\frac{\partial u}{\partial x}+K_{22}\frac{\partial u}{\partial y}+D_{21}\frac{\partial v}{\partial x}+D_{22}\frac{\partial v}{\partial y}=0,\quad \text{at}\quad y=\pm L_y. \tag{18}$$

Boundary conditions of type 1 correspond to those employed in the isotropic media, namely, diagonal $\mathbf{k}$ and $\mathbf{D}$ when there are no cross-diffusion terms, i.e. when $\mathbf{d}=\mathbf{K}=0$. Equations (6) and (7) set the normal gradient of u and v to the boundaries equal to zero and ignore cross-diffusion effects, whereas equations (9), (10), (13), (14), (17) and (18) set the total fluxes of heat and species mass fractions normal to the boundaries equal to zero. Finally, equations (11) and (12) set part of the total fluxes of heat and species mass fractions normal to the boundaries equal to zero. In the theory of transport phenomena, the most accurate and realistic boundary conditions are those of equations (17) and (18), whilst the rest are approximations. As stated in the Introduction, one of the objectives of this paper is to determine the effects of the boundary conditions on two-dimensional, anisotropic, reactive-diffusive systems.

3. Numerical method

Upon discretization of the time derivative in equation (1) by means of a θ-method, linearization of the resulting partial differential equations with respect to the previous time step and factorization of the resulting equation, one can easily obtain

$$\left(\mathbf{I}-\theta\Delta t\alpha\frac{\partial^2}{\partial x^2}-\theta\Delta t\delta\mathbf{J}\right)\left(\mathbf{I}-\theta\Delta t\gamma\frac{\partial^2}{\partial y^2}-\theta\Delta t\varepsilon\mathbf{J}\right)\Delta\mathbf{U}$$

$$=\mathbf{RHS}+\theta\Delta t\beta\frac{\partial^2\Delta\mathbf{U}}{\partial x\,\partial y}+\mathbf{AFE}, \tag{19}$$

where $\mathbf{I}$ is the 2×2 identity matrix, $\Delta\mathbf{U}=\mathbf{U}^{n+1}-\mathbf{U}^n$, $\delta+\varepsilon=1$, $\mathbf{J}=\partial\mathbf{S}/\partial\mathbf{U}$ denotes the Jacobian matrix, Δt is the time step, n denotes the n-th time level, i.e. $t^n=n\Delta t$ and $n=0,1,2,\ldots$, θ is the implicitness parameter, i.e. $0\leq\theta\leq 1$,

$$\mathbf{RHS}=\Delta t\left(\alpha\frac{\partial^2\mathbf{U}^n}{\partial x^2}+\beta\frac{\partial^2\mathbf{U}^n}{\partial x\,\partial y}+\gamma\frac{\partial^2\mathbf{U}^n}{\partial y^2}+\mathbf{S}(\mathbf{U}^n)\right), \tag{20}$$

and the approximate factorization errors can be expressed as

$$\mathbf{AFE}=\Delta t^2\theta^2\left(\alpha\frac{\partial^2}{\partial x^2}\left(\gamma\frac{\partial^2\Delta\mathbf{U}}{\partial y^2}\right)+\varepsilon\alpha\frac{\partial^2}{\partial x^2}(\mathbf{J}\Delta\mathbf{U})+\delta\mathbf{J}\gamma\frac{\partial^2\Delta\mathbf{U}}{\partial y^2}+\delta\varepsilon\mathbf{J}^2\Delta\mathbf{U}\right). \tag{21}$$

The second-order spatial derivatives that appear in equations (19) and (20) have been discretized by means of the second-order accurate formulae as

$$\left(\frac{\partial^2 \mathbf{U}}{\partial x^2}\right)_{i,j} = \frac{1}{\Delta x^2}\delta_x^2 \mathbf{U}_{i,j} + O(\Delta x^2), \tag{22}$$

$$\left(\frac{\partial^2 \mathbf{U}}{\partial y^2}\right)_{i,j} = \frac{1}{\Delta y^2}\delta_y^2 \mathbf{U}_{i,j} + O(\Delta x^2), \tag{23}$$

$$\left(\frac{\partial^2 \mathbf{U}}{\partial x\,\partial y}\right)_{i,j} = \frac{1}{4\Delta x \Delta y}\delta_{xy}^2 \mathbf{U}_{i,j} + O(\Delta x^2, \Delta y^2), \tag{24}$$

where $\delta_x^2 \mathbf{U}_{i,j} = \mathbf{U}_{i+1,j} - 2\mathbf{U}_{i,j} + \mathbf{U}_{i-1,j}$, $\delta_y^2 \mathbf{U}_{i,j} = \mathbf{U}_{i,j+1} - 2\mathbf{U}_{i,j} + \mathbf{U}_{i,j-1}$ and $\delta_{xy}^2 \mathbf{U}_{i,j} = \mathbf{U}_{i+1,j+1} - \mathbf{U}_{i+1,j-1} - \mathbf{U}_{i-1,j+1} + \mathbf{U}_{i-1,j-1}$, and the subscripts i and j denote the coordinates x_i and y_j, respectively, of the grid points.

In this paper, we consider $\delta = \varepsilon = {}^1/_2$ and a trapezoidal rule, i.e. $\theta = {}^1/_2$, which is second-order accurate in time, and neglect the second-order approximate factorization errors in equation (19). However, the presence of the mixed second-order derivative terms in equation (19) does not allow for an exact factorization. As a consequence, these mixed second-order derivative terms have frequently been treated explicitly, especially in Computational Fluid Dynamics (CFD), i.e. the mixed second-order derivative terms in the right-hand side of equation (19) have frequently been set to zero, or have been approximated by explicit second-order accurate formulae involving two previous time levels (Beam and Warming, 1978; Briley and McDonald, 2001; Steinthorsson *et al.*, 1991). In this paper, we account for the mixed second-order derivative terms in equation (19) by means of a generalization of the iterative predictor-corrector strategy developed by the author for isotropic reactive-diffusive media (Ramos, 1999) as follows. In the predictor (P) step, the following one-dimensional operators are solved

$$\mathbf{L}_x(\Delta \mathbf{U}^{*P}) \equiv \left(\mathbf{I} - \frac{\theta \Delta t}{\Delta x^2}\alpha \delta_x^2 - \theta \Delta t \delta \mathbf{J}\right)(\Delta \mathbf{U}^{*P}) = \mathbf{RHS}, \tag{25}$$

$$\mathbf{L}_y(\Delta \mathbf{U}) \equiv \left(\mathbf{I} - \frac{\theta \Delta t}{\Delta y^2}\gamma \delta_y^2 - \theta \Delta t \varepsilon \mathbf{J}\right)(\Delta \mathbf{U}^{P}) = \Delta \mathbf{U}^{*P}, \tag{26}$$

where **RHS** has been discretized as per equations (22)-(24), and the superscript P denotes the predictor step. In this step, the mixed second-order derivative terms that appear in equation (19) are neglected, i.e. the mixed second-order derivative terms are treated explicitly; as a consequence, equations (25) and (26) are linear and decoupled, and can be solved sequentially to determine the predictor solution.

In the corrector (C) step, the following linear one-dimensional operators are solved

$$\mathbf{L}_x(\Delta\mathbf{U}^{*k}) = \mathbf{RHS} + \theta\Delta t\beta\frac{\partial^2\Delta\mathbf{U}^{k-1}}{\partial x\,\partial y}, \quad k = 1, 2, \ldots, \tag{27}$$

$$\mathbf{L}_y(\Delta\mathbf{U}^{k}) = \Delta\mathbf{U}^{*k}, \quad k = 1, 2, \ldots, \tag{28}$$

where k denotes the k-th iteration within the time step, and the second term in the right-hand side of equation (27) for $k = 1$ is that of the predictor step.

The solutions of the one-dimensional equations (27) and (28) require the use of boundary conditions. Since the most general boundary conditions considered in this paper are those of type 5, i.e. equations (15)-(18), we shall only write the boundary conditions for the one-dimensional operators of equations (27) and (28) for these boundary conditions. Note that the boundary conditions of types 1-4 can be easily obtained from those of type 5.

From equations (15) and (16), it can be easily deduced that

$$\frac{\partial\mathbf{U}}{\partial x} = -\mathbf{A}_L\frac{\partial\mathbf{U}}{\partial y}, \quad \text{at} \quad x = -L_x, \tag{29}$$

$$\frac{\partial\mathbf{U}}{\partial x} = -\mathbf{A}_R\frac{\partial\mathbf{U}}{\partial y}, \quad \text{at} \quad x = +L_x, \tag{30}$$

provided that $k_{11}D_{11} - d_{11}K_{11} \neq 0$, whereas, from equations (17) and (18), one can obtain

$$\frac{\partial\mathbf{U}}{\partial y} = -\mathbf{A}_B\frac{\partial\mathbf{U}}{\partial x}, \quad \text{at} \quad y = -L_y, \tag{31}$$

$$\frac{\partial\mathbf{U}}{\partial y} = -\mathbf{A}_T\frac{\partial\mathbf{U}}{\partial x}, \quad \text{at} \quad y = +L_y, \tag{32}$$

provided that $k_{22}D_{22} - d_{22}K_{22} \neq 0$, where $\mathbf{A}_L$, $\mathbf{A}_R$, $\mathbf{A}_B$ and $\mathbf{A}_T$ are (constant) matrices, the components of which can be easily deduced from equations (15) and (16) and equations (17) and (18), respectively.

Equations (29)-(32) can be written in delta form using the terminology of the iterative predictor-corrector method described above as

$$\frac{\partial\Delta\mathbf{U}^{*k}}{\partial x} = -\mathbf{A}_L\frac{\partial\Delta\mathbf{U}^{k-1}}{\partial y}, \quad \text{at} \quad x = -L_x, \tag{33}$$

$$\frac{\partial \Delta \mathbf{U}^{*k}}{\partial x} = -\mathbf{A}_R \frac{\partial \Delta \mathbf{U}^{k-1}}{\partial y}, \quad \text{at} \quad x = +L_x, \tag{34}$$

$$\frac{\partial \Delta \mathbf{U}^{k}}{\partial y} = -\mathbf{A}_B \frac{\partial \Delta \mathbf{U}^{*k}}{\partial x}, \quad \text{at} \quad y = -L_y, \tag{35}$$

$$\frac{\partial \Delta \mathbf{U}^{k}}{\partial y} = -\mathbf{A}_T \frac{\partial \Delta \mathbf{U}^{*k}}{\partial x}, \quad \text{at} \quad y = +L_y, \tag{36}$$

for $k = 1, 2, \ldots$, with $\partial \Delta \mathbf{U}^{*k}/\partial x = 0$ at $x = \pm L_x$ for $k = 1$, and can be discretized by means of second-order accurate formulae using fictitious points. The discrete values of the dependent variables at the fictitious points can then be written in terms of the values of the dependent variables at the boundaries and points next to the boundaries, and can be substituted into the second-order accurate discretizations of equations (27) and (28) at the boundaries in order to obtain a system of linear algebraic equations with block-tridiagonal matrices for all the interior and boundary points. These block-tridiagonal systems of linear algebraic equations can be solved efficiently by means of LU decomposition.

3.1 Convergence of the iterative predictor-corrector method

In order to analyze the convergence properties of the iterative predictor-corrector method, it is convenient to introduce the following variables

$$\boldsymbol{\rho}^k = \Delta \mathbf{U} - \Delta \mathbf{U}^k, \quad \boldsymbol{\rho}^k = \Delta \mathbf{U}^* - \Delta \mathbf{U}^{*k}, \tag{37}$$

so that subtraction of equations (27) and (28) from the same equations, but without the superscripts k and $k - 1$ yields

$$\mathbf{L}_y(\boldsymbol{\rho}^k) = \boldsymbol{\mu}^k, \tag{38}$$

$$\mathbf{L}_x(\boldsymbol{\mu}^k) = \theta \Delta t \beta \frac{\partial^2 \boldsymbol{\rho}^{k-1}}{\partial x \, \partial y}, \tag{39}$$

which, upon substitution of equations (22)-(24) and $\rho_{i,j}^k = \phi^k \exp(I(k_x x_i + k_y y_j))$, result in

$$\mathbf{M}\boldsymbol{\phi}^k = \mathbf{N}\boldsymbol{\phi}^{k-1}, \tag{40}$$

where $I^2 = -1$, k_x and k_y denote the wavenumbers in the x and y directions, respectively, and

$$\mathbf{M}=\left(\mathbf{I}+4\frac{\theta\Delta t}{\Delta x^2}\alpha\sin^2\frac{k_x\Delta x}{2}-\theta\delta t\,\delta\mathbf{J}\right)\left(\mathbf{I}+4\frac{\theta\Delta t}{\Delta y^2}\gamma\sin^2\frac{k_y\Delta y}{2}-\theta\delta t\varepsilon\mathbf{J}\right), \quad (41)$$

$$\mathbf{N}=-\frac{\theta\Delta t}{\Delta x\,\Delta y}\beta\sin k_x\Delta x\sin k_y\Delta y. \quad (42)$$

A necessary condition for the convergence of the iterative predictor-corrector method is that $\|\mathbf{M}^{-1}\mathbf{N}\|$ be less than unity, and this norm depends clearly on the time step, the diffusion tensors **k**, **K**, **d** and **D**, the Jacobian matrix **J**, the implicitness parameter θ, the allocation of the reaction terms to the x and y operators, and the step sizes in the x and y directions. In addition, the necessary condition for convergence was established without considering the boundary conditions.

The following convergence criterion was employed to determine the convergence of the iterative method presented in this paper

$$\left(\frac{(\Delta\mathbf{U}^{k+1}-\Delta\mathbf{U}^{k})^{\mathrm{T}}\cdot(\Delta\mathbf{U}^{k+1}-\Delta\mathbf{U}^{k})}{N_xN_y}\right)^{\frac{1}{2}}\leq 10^{-8}, \quad (43)$$

where

$$\mathbf{U}^{\mathrm{T}}\cdot\mathbf{U}=\sum_{i=1}^{N_x}\sum_{j=1}^{N_y}\left(u_{i,j}^2+v_{i,j}^2\right), \quad (44)$$

N_x and N_y are the number of grid points in the x and y directions, respectively.

3.2 Linear stability of the approximate factorization method

In order to analyze the linear stability of the linear, implicit, approximate factorization method presented above, it is convenient to introduce the following variables

$$\mathbf{U}_{i,j}^{n}=\psi^{n}\exp\left(I(k_xx_i+k_yy_j)\right), \quad (45)$$

which, upon being substituted into equation (19) without the approximate factorization errors, using equations (22)-(24) and assuming that **S** is a linear function of **U**, i.e. $\mathbf{S}=\mathbf{J}\mathbf{U}$, where **J** is a constant matrix, yields

$$\mathbf{P}\psi^{k}=\mathbf{Q}\psi^{k-1}, \quad (46)$$

where

$$\mathbf{P} = \left(\mathbf{I} + 4\frac{\theta\Delta t}{\Delta x^2}\alpha\sin^2\frac{k_x\Delta x}{2} - \theta\delta t\,\delta\mathbf{J}\right)\left(\mathbf{I} + 4\frac{\theta\Delta t}{\Delta y^2}\gamma\sin^2\frac{k_y\Delta y}{2} - \theta\delta t\varepsilon\mathbf{J}\right) + \frac{\Delta t}{\Delta x\,\Delta y}\beta\sin k_x\Delta x\sin k_y\Delta y, \tag{47}$$

$$\mathbf{Q} = \mathbf{P} + \Delta t\mathbf{J} - 4\frac{\Delta t}{\Delta x^2}\alpha\sin^2\frac{k_x\Delta x}{2} - 4\frac{\Delta t}{\Delta y^2}\gamma\sin^2\frac{k_y\Delta y}{2} + \frac{\Delta t}{\Delta x\,\Delta y}\beta\sin k_x\Delta x\sin k_y\Delta y. \tag{48}$$

A necessary condition for linear stability is that the norm of the matrix $\mathbf{P}^{-1}\mathbf{Q}$ be less than unity, and this norm depends clearly on the time step, the diffusion tensors **k**, **K**, **d** and **D**, the (constant) Jacobian matrix **J**, the implicitness parameter θ, the allocation of the reaction terms to the x and y operators, i.e. δ and ε, and the step sizes in the x and y directions. In addition, the necessary condition for linear or Fourier-von Neumann stability was established without considering the boundary conditions.

4. Presentation of results

As indicated in Section 2, for a specified reaction mechanism, time-dependent reaction-diffusion processes in two-dimensional, anisotropic media are characterized by a large set of parameters, i.e. the four components each of the heat and species diffusion tensors **D** and **k**, respectively, and the four components each of the cross-diffusion terms **K** and **d**, i.e. 16 diffusion coefficients. In addition, five different boundary conditions have been employed in this study; therefore, a detailed numerical study of the time-dependent reaction-diffusion processes in two-dimensional anisotropic media requires a large set of simulations. Moreover, grid independence studies require that simulations be performed with different time steps and spatial step sizes so that the results are independent of the time step and mesh dimensions. Such a large number of simulations may pose a problem when the results are to be presented in a concise and understandable manner. In order to avoid such a presentation problem as much as possible, this section has been organized in different subsections dealing with grid independent studies, the effects of anisotropy on the temperature and species, the effects of cross-diffusion processes and the effects of the boundary conditions on the results. But even with such an organization, the large number of simulations that have been performed force us to present only the most relevant results and make comments on other results that, for brevity, are not reported here.

The effects of the boundary conditions and Soret and Dufour effects on the reactive-diffusive phenomena in two-dimensional anisotropic media have been

assessed by means of three-dimensional plots of u and v at selected times, time histories of u and v at four monitoring locations and the profiles of u and v along the x and y axes at selected times. The time history profiles allow us to determine the arrival time of the propagating front at a specified location, whereas the profiles along the x and y axes allow us to observe the symmetry characteristics of the u and v profiles at selected times.

A summary of some of the parameters used in the calculations are shown in Table I. Case 1 of this table corresponds to the isotropic heat and species diffusion, i.e. isotropic **k** and **D**, without the effects of heat diffusion on species mass diffusion (Soret effect), i.e. $\mathbf{d} = 0$, and the effects of species mass diffusion

Case	k_{11}	k_{12}	k_{21}	k_{22}	d_{11}	d_{12}	d_{21}	d_{22}	K_{11}	K_{12}	K_{21}	K_{22}	D_{11}	D_{12}	D_{21}	D_{22}
1	1	0	0	1	0	0	0	0	0	0	0	0	1	0	0	1
2	1	0.5	0	1	0	0	0	0	0	0	0	0	1	0	0	1
3	1	1	0	1	0	0	0	0	0	0	0	0	1	0	0	1
4	1	0	0.5	1	0	0	0	0	0	0	0	0	1	0	0	1
5	1	0	1	1	0	0	0	0	0	0	0	0	1	0	0	1
6	1	0.5	0.5	1	0	0	0	0	0	0	0	0	1	0	0	1
7	1	0	0	1	0	0	0	0	0	0	0	0	1	0.5	0	1
8	1	0	0	1	0	0	0	0	0	0	0	0	1	1	0	1
9	1	0	0	1	0	0	0	0	0	0	0	0	1	0	0.5	1
10	1	0	0	1	0	0	0	0	0	0	0	0	1	0	1	1
11	1	0	0	1	0	0	0	0	0	0	0	0	1	0.5	0.5	1
12	1	0	0	1	0.5	0	0	0.5	0	0	0	0	1	0	0	1
13	1	0	0	1	0.5	0.1	0.1	0.5	0	0	0	0	1	0	0	1
14	1	0	0	1	0.5	0.5	0.5	0.5	0	0	0	0	1	0	0	1
15	1	0	0	1	0	0	0	0	0.1	0	0	0	1	0	0	1
16	1	0	0	1	0	0	0	0	0	0	0	0.1	1	0	0	1
17	1	0	0	1	0	0	0	0	0.1	0	0	0.1	1	0	0	1
18	1	0	0	1	0	0	0	0	0	0.1	0	0	1	0	0	1
19	1	0	0	1	0	0	0	0	0	0	0.1	0	1	0	0	1
20	1	0	0	1	0.5	0	0	0.5	0.1	0	0	0.1	1	0	0	1
21	1	0	0	1	0.5	0.5	0.5	0.5	0.1	0	0	0.1	1	0	0	1
22	1	0	0	1	0.5	0	0	0.5	0.1	0.1	0.1	0.1	1	0	0	1
23	1	0	0	1	0.5	0.5	0.5	0.5	0.1	0.1	0.1	0.1	1	0	0	1
24	1	0.4	0.4	1	0.5	0	0	0.5	0.1	0	0	0.1	1	0	0	1
25	1	0.4	0.4	1	0.5	0.1	0.1	0.5	0.1	0	0	0.1	1	0	0	1
26	1	0.4	0.4	1	0.5	0	0	0.5	0.1	0.1	0.1	0.1	1	0	0	1
27	1	0.4	0.4	1	0.5	0.5	0.5	0.5	0.1	0.1	0.1	0.1	1	0	0	1
28	1	0.4	0.4	1	0.5	0	0	0.5	0.1	0	0	0.1	1	0	0	1
29	1	0	0	1	0.5	0	0	0.5	0.1	0	0	0.1	1	0.4	0.4	1
30	1	0	0	1	0.5	0.5	0.5	0.5	0.1	0	0	0.1	1	0.4	0.4	1
31	1	0	0	1	0.5	0	0	0.5	0.1	0.1	0.1	0.1	1	0.4	0.4	1

Table I.
Components of the diffusivity tensors **k**, **d**, **K** and **D**

on heat diffusion (Dufour effect), i.e. $\mathbf{K} = 0$. Cases 2-6 correspond to the anisotropic species diffusion and isotropic heat diffusion without cross-diffusion effects. In cases 7-11, the species diffusion is isotropic, heat diffusion is anisotropic and there are no Soret and Dufour processes, whereas, in cases 12-14, the species and heat diffuse isotropically and there is thermodiffusion, but there are no Soret effects. In cases 15-19, species and heat diffuse isotropically, and there are Soret effects, but there is no thermodiffusion. In cases 20-23, heat and species diffuse isotropically but there are Soret and Dufour effects, whereas, in cases 24-31, there is cross-diffusion of the species and heat, the heat diffuses anisotropically in cases 24-28, and the species diffuse anisotropically in cases 29-31.

It must be pointed out that the tensors $\mathbf{k}$ and $\mathbf{D}$ considered here are positive definite, so that, for example, $(k_{12} + k_{21})^2 < 4k_{11}k_{22}$; therefore, in the absence of cross-diffusion effects and under steady state conditions, equations (1) and (2) are elliptic.

4.1 General considerations and grid-independence studies

Before presenting some sample results for anisotropic media, it seems convenient to review what has been observed in isotropic media with $\mathbf{d} = \mathbf{K} = 0$, and diagonal $\mathbf{k}$ and $\mathbf{D}$ with identical (diagonal) components equal to one, i.e. case 1 of Table I, so that the anisotropic results can be compared with the isotropic ones, and to discuss the grid-independent studies that have been performed.

In case 1, it has been observed that the initial condition in v results in the formation of a peak in v (Figure 1) and a valley in u (Figure 2). The peak in v decreases in amplitude, whereas its width increases as time increases; eventually, a valley is formed in the center of the domain as shown in the fourth frame of Figure 1, the depth and width of which increase until the reaction front approaches the boundaries of the domain. Later on, the values of v at the boundaries of the domain increase (sixth frame) and exceed those in the interior of the domain (frames 8 and 9 of Figure 2), before a steady state is reached. It must be noted that the calculations shown in Figure 1 were performed with a 101×101-point mesh and $\Delta t = 0.04$, but only 50×50 points have been drawn in Figures 1 and 2 for clarity, and that the solution at $t = 50$ is not the steady state one.

The valley exhibited by u (Figure 2) also spreads sideways, the value of u at the boundaries decreases below its initial condition at a faster pace than those at the corners of the domain (frames 5-8), and, at $t = 50$, is smaller than those in the middle of the computational domain (frame 9). The results presented in Figures 1 and 2 indicate that both v and u are symmetric with respect to the x and y axes, as one should expect. This symmetry is lost whenever the diffusivity tensors are anisotropic as shown in Figures 3 and 4 which correspond to the case 6 of Table I and present snapshots of u and v,

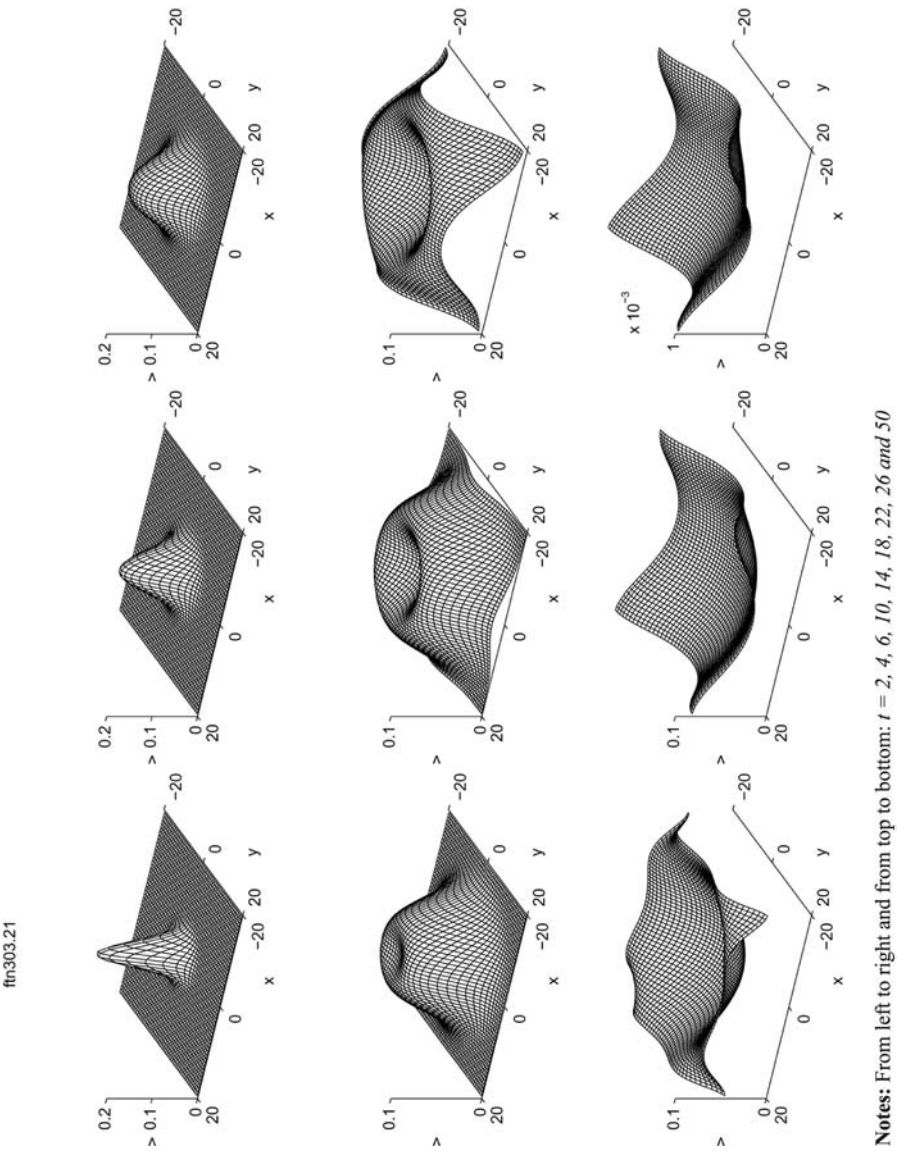

Figure 1.
v at selected times for case 1 of Table I and boundary conditions of type 1

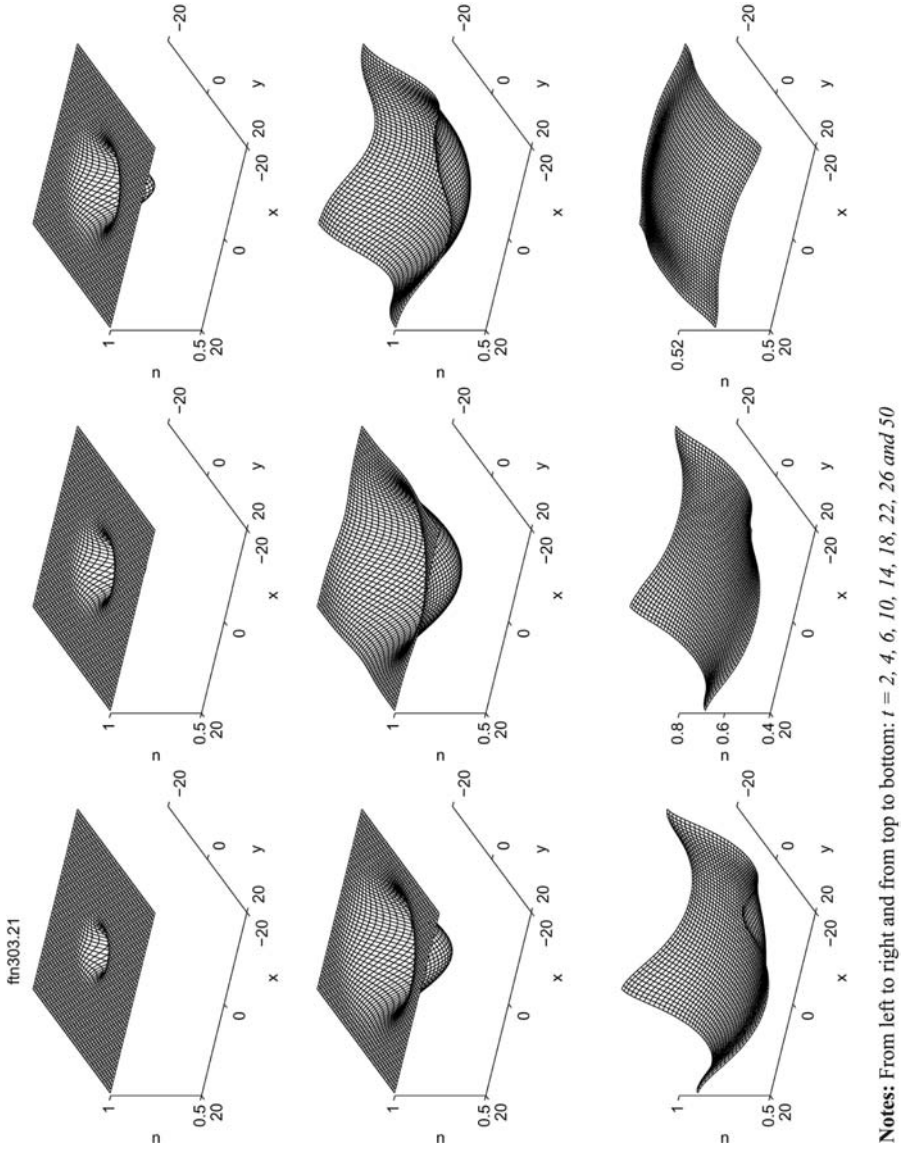

Notes: From left to right and from top to bottom: $t = 2, 4, 6, 10, 14, 18, 22, 26$ *and* 50

Figure 2.
u at selected times for case 1 of Table I and boundary conditions of type 1

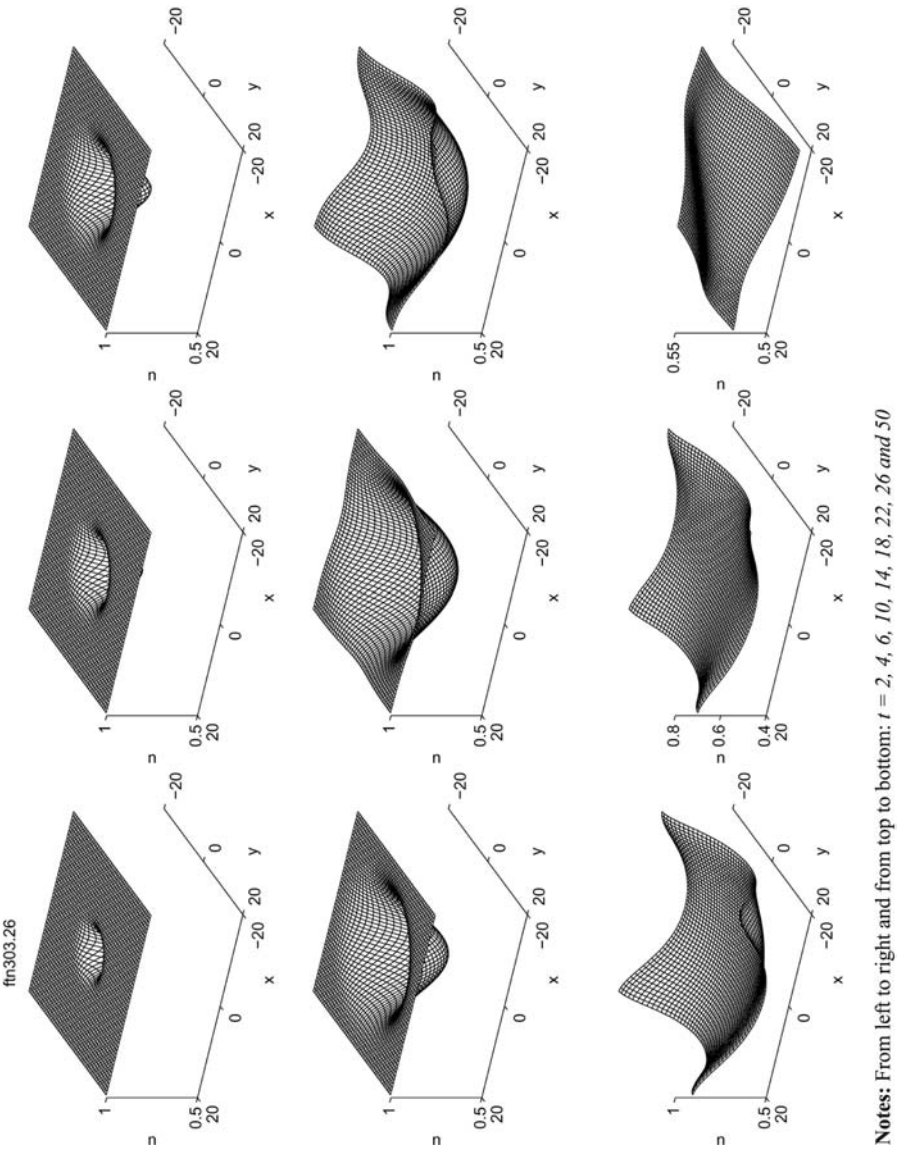

Figure 3.
u at selected times for case 6 of Table I and boundary conditions of type 1

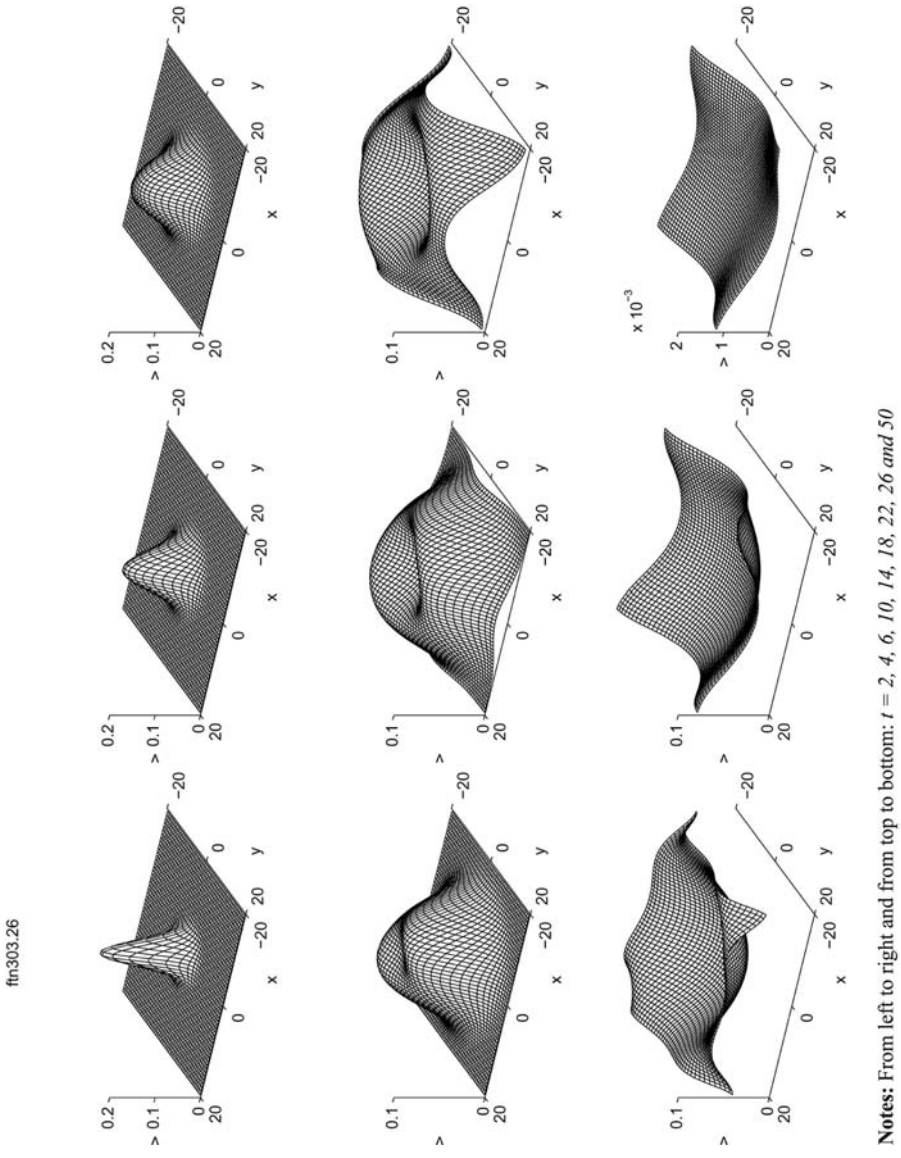

Notes: From left to right and from top to bottom: $t = 2, 4, 6, 10, 14, 18, 22, 26$ *and* 50

Figure 4.
v at selected times for case 6 of Table I and boundary conditions of type 1

respectively, at selected times. For example, the effects of the anisotropy in the diffusion of species can be observed if Figure 3 is compared with Figure 2. In particular, Figure 3 shows that the width of the valley in u is larger along the diagonal that connects the corners located at $(-20, -20)$ and $(20, 20)$ than along the other diagonal in the first to fifth frames of this figure. The sixth and seventh frames of Figure 3 indicate that the reaction front reaches the corners located at $(-20, -20)$ and $(20, 20)$ earlier than those at $(-20, 20)$ and $(20, -20)$ where the value of u is nearly the same as the initial condition. Later on, the last two frames of Figure 3 indicate that the values of u at the corners located at $(-20, -20)$ and $(20, 20)$ decrease.

The results presented in Figure 4 show that the v-front reaches the corners located at $(20, 20)$ and $(-20, -20)$ earlier than those located at $(20, -20)$ and $(-20, 20)$; the value of v at the latter is nearly identical to the initial value of v before the front reaches these corners. At larger times, the results presented in the ninth frame of Figure 4 indicate that the maximum values of v occur near the corners located at $(-20, 20)$ and $(20, -20)$ on account of the species and heat transport processes.

The results presented in Figures 1-4 indicate that the reaction front is characterized by steep gradients of u and v as it approaches, but is far from the boundaries. Once this front is near the boundaries, the magnitude of the gradients there decreases as a consequence of the homogeneous Neumann boundary conditions employed in this study.

All the cases 1-31 of Table I and other studies not presented here were performed with meshes consisting of 101×101, 201×201 and 401×401 points, and it was observed that the largest absolute value of the (local) difference between the results corresponding to 101×101 and 201×201-point meshes was less than 10^{-6} in u and v for $\Delta t = 0.01$, whereas the largest (local) difference between the results corresponding to 201×201 and 401×401-point meshes was less than 10^{-7} in u and v for the same step. The time at which the largest difference was observed, was found to depend on the heat and species diffusion tensors and the Soret and Dufour effects.

For a 101×101-point mesh, it was found that the local errors decreased quadratically as the time step was decreased from $\Delta t = 0.04$ to 0.001, and that the largest difference between the results corresponding to $\Delta t = 0.04$ to 0.01 was on the order of 10^{-5} for cases 1-11 of Table I. Therefore, $\Delta t = 0.04$ was employed for cases 1-11, whereas Δt was equal to 0.01, 0.005 and 0.0001 for cases 12-19, 20-23 and 24-31, respectively. Cases 12-31 were found to require smaller time steps due to cross-diffusion effects which increase the norm of the matrices that guarantee the convergence of the iterative predictor-corrector strategy and the linear stability of the approximate factorization method employed in this paper (cf. Section 3).

4.2 Effect of the species diffusion anisotropy

As shown in Figures 3 and 4 which correspond to case 6, it has been observed that the reactive front approaches earlier the corners located at (20, 20) and $(-20, -20)$ than the other two corners, although it is difficult to notice the differences between the three-dimensional plots of, say, Figures 1 and 2 and the corresponding figures for case 6 with the naked eyes. For this reason and in order to assess the effects of anisotropy on the motion of the reacting fronts in cases 1-31 and, in particular, in Figures 1-4, we have monitored the values of u and v as functions of time at the locations $(x, y) = (1.60, 1.60)$, $(-10.4, 9.60)$, $(9.60, -10.4)$ and $(9.60, 9.60)$ in order to determine the arrival time of the reacting front at these locations.

For cases 1-6, where there are no Soret and Dufour effects, heat diffuses isotropically and the species diffusivity tensor is anisotropic, the time histories shown in Figure 5 indicate that, at the location (9.60, 9.60), there are very few differences in the u profiles for cases 1-4, and cases 3-6 result in a slightly thicker u profile at $t = 50$ than case 1; the results of case 4 are indistinguishable from those of cases 2 and 3 in Figure 5. Similar trends to those of cases 2 and 4 are observed for cases 5 and 6.

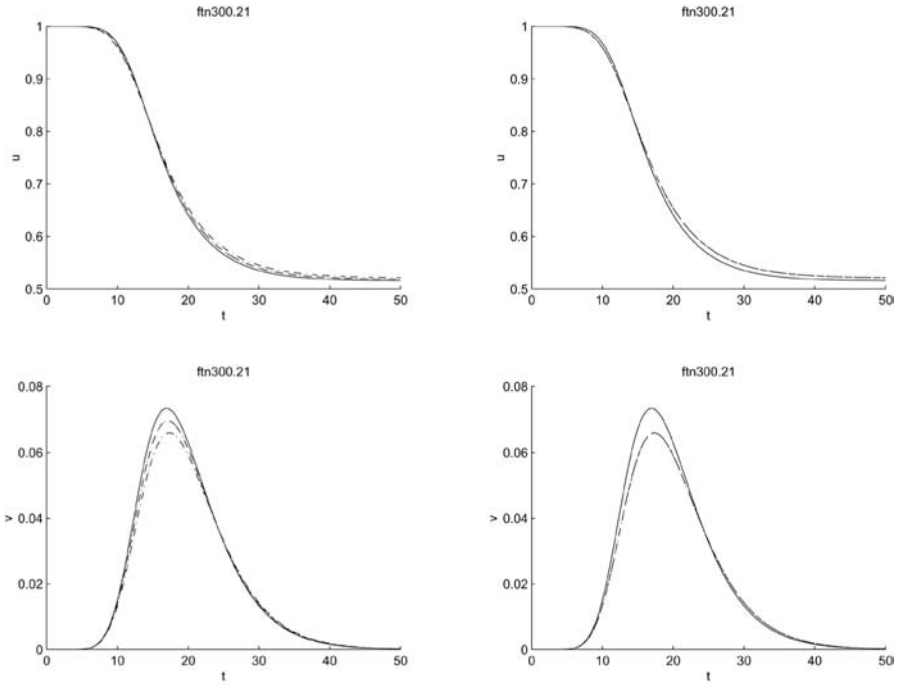

Notes: Left: solid line = case 1; dashed line = case 2; dashed-dotted line = case 3; dotted line = case 4. Right: solid line = case 1; dashed line = case 5; dashed-dotted line = case 6

Figure 5.
Time histories of u (top) and v (bottom) at $(x, y) = (9.60, 9.60)$ for boundary conditions of type 1

The time histories of v shown in Figure 5 indicate that case 1 results in a larger maximum value of v than cases 2-6.

Another illustration of the effects of species diffusion anisotropy on two-dimensional reaction-diffusion phenomena is shown in Figure 6 which exhibits the profiles of u and v along the x and y axes for cases 1-6 at $t = 50$. This figure indicates that the effects of the anisotropy of the species diffusivity tensor on the symmetry of the u and v profiles is small for cases 1-6, although cases 2, 4-6 results in a larger maximum value of u than cases 1 and 3 and, for the anisotropic cases 2-6, the values of u and v at the boundaries located at $x = L_x$ and $y = L_y$ are larger than those at $x = -L_x$ and $y = -L_y$ in accordance with the three-dimensional plots presented in Figures 3 and 4.

In order to understand the results presented in Figures 3-6, it is convenient to consider the principal directions of the tensor **k**. We shall consider, as an example, an orthotropic tensor with $k_{11} = k_{12} = 1$ and $k_{12} = k_{21}$. For such a tensor which includes the isotropic one, it can be easily shown that its eigenvalues are $1 \pm k_{12}$ and its principal or main directions are $(1, 1)^T$ and $(-1, 1)^T$, and the tensor can be diagonalized. This implies that, along the $(1, 1)^T$-direction the species diffusivity is larger than along the

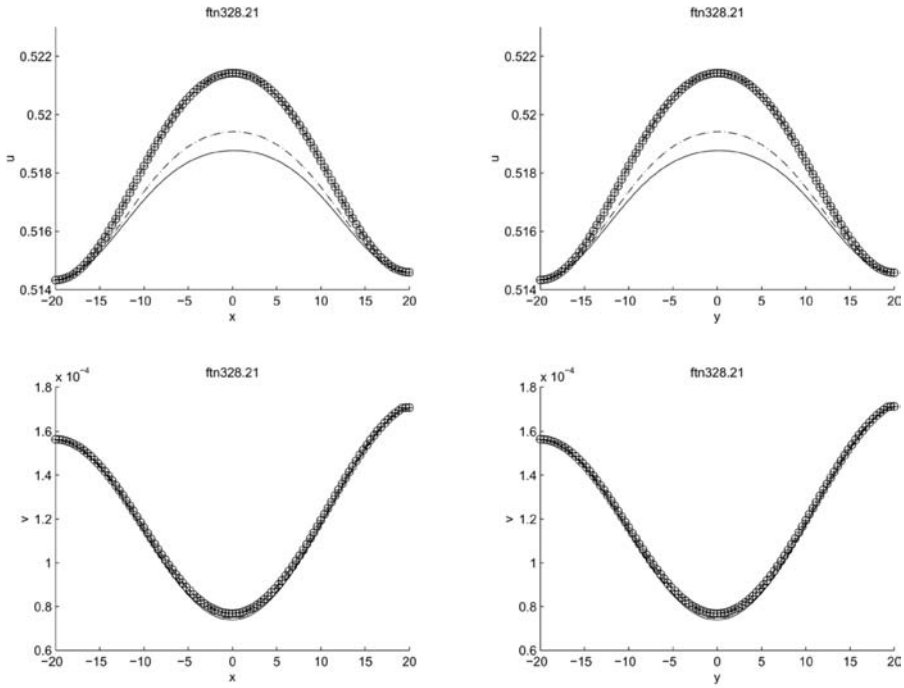

Figure 6.
$u(x,0, 50)$ and $v(x,0, 50)$ (left) and $u(0, y, 50)$ and $v(0, y, 50)$ (right) for boundary conditions of type 1

Notes: Left: solid line = case 1; dashed line = case 2; dashed-dotted line = case 3; dotted line = case 4 cross = case 5; circle = case 6

$(1, -1)^{T}$-direction and, as a consequence, the species diffuse at a faster rate along the former direction and the rate of diffusion increases as k_{12} increases. Since for cases 2-6, heat diffuses isotropically and there are no Soret and Dufour effects, one should expect a higher diffusion and faster reaction along the $(1, 1)^{T}$-direction than along the $(1, -1)^{T}$-direction as indicated in the u and v-profiles shown along the x and y axes in Figure 6.

4.3 Effect of the heat diffusion anisotropy

The effect of the anisotropy of the heat diffusion tensor, **D**, is illustrated in the time histories shown in Figure 7 which indicate that case 1 predicts a slower propagating front than cases 7-11, cases 10 and 11 yield nearly the same results, and the results of case 9 are indistinguishable from those of case 7. The slowness of the u and v profiles observed in Figure 7 for case 1 indicates that the anisotropy of the heat diffusion tensor results in a maximum value of v larger than that for an isotropic heat diffusivity tensor, i.e. case 1.

Figure 8 shows that the effects of the anisotropy of the heat diffusivity tensor on the symmetry of the u and v profiles along the x and y axes are small. However, cases 7 and 9-11 result in a larger maximum value of u than cases 1

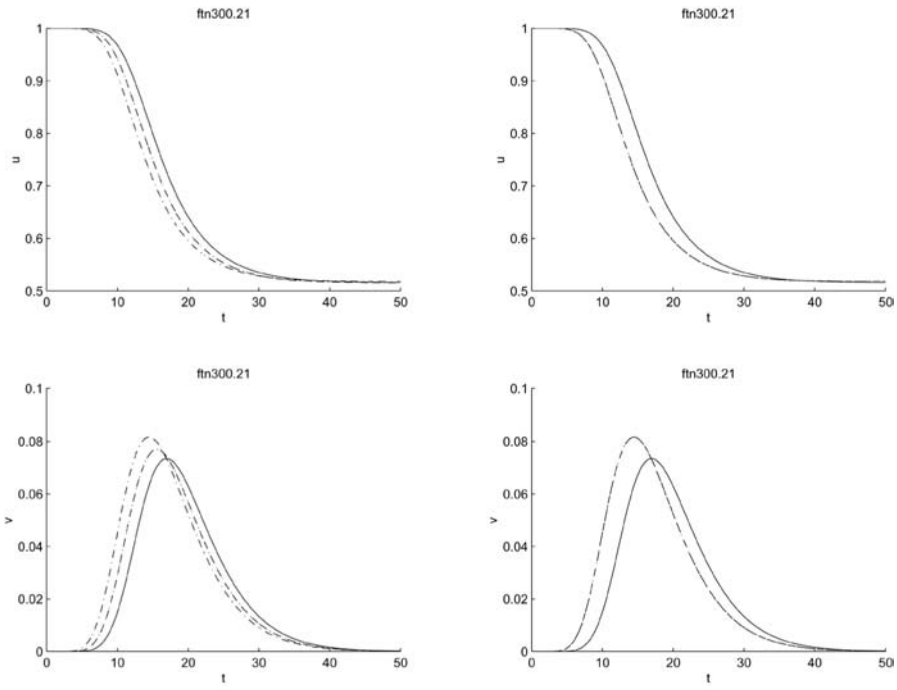

Notes: Left: solid line = case 1; dashed line = case 7; dashed-dotted line = case 8; dotted line = case 9
Right: solid line = case 1; dashed line = case 10; dashed-dotted line = case 11

Figure 7.
Time histories of u (top) and v (bottom) at $(x, y) = (9.60, 9.60)$ for boundary conditions of type 1

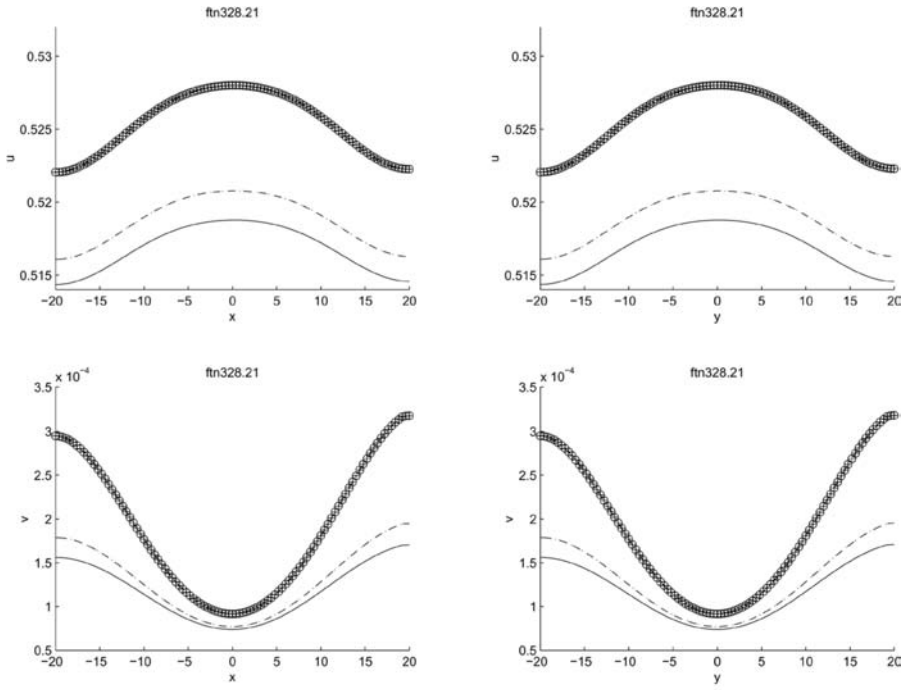

Figure 8.
$u(x, 0, 50)$ and $v(x, 0, 50)$ (left) and $u(0, y, 50)$ and $v(0, y, 50)$ (right) for boundary conditions of type 1

Notes: Left: solid line = case 1; dashed line = case 7; dashed-dotted line = case 8; dotted line = case 9; cross = case 10; circle = case 11

and 8; therefore, the maximum value of u along the x and y axes increases as the anisotropy of **D** is increased. Furthermore, cases 7 and 9-11 yield larger values of u and v at the boundaries located at $x = L_x$ and $y = L_y$ than at $x = -L_x$ and $y = -L_y$, and these values are larger than those predicted by cases 1 and 8.

The results shown in Figures 7 and 8 can be readily explained in terms of the principal directions and eigenvalues of the diffusivity tensor **D** as indicated in the previous subsection. Thus, in case 11, the eigenvalues of this tensor are 1.5 and 0.5 and their corresponding eigenvectors are $(1, 1)^{\mathrm{T}}$ and $(1, -1)^{\mathrm{T}}$; therefore, one should expect an increased reaction rate and faster propagating front along $(1, 1)^{\mathrm{T}}$ than along $(1, -1)^{\mathrm{T}}$, and this corresponds precisely to the results shown in Figures 7 and 8, although the effects of the anisotropy heat diffusion tensor are small.

4.4 The Soret effect

The Soret effect in the absence of the Dufour one and with isotropic heat and species diffusion is illustrated in the time histories of u and v shown in Figure 9. This figure clearly indicates that, for the parameters listed in cases 12-14 of Table I and the reaction mechanism considered in this paper, the Soret effect is

small and results in slightly faster and thinner propagating fronts than the isotropic case 1.

The u and v profiles along the x and y axes shown in Figure 10 clearly indicate that the anisotropy of these profiles is largest for cases 13 and 14 which correspond to a full and symmetric **d** tensor, the differences in the u and v profiles between cases 13 and 14 are small. Almost the same asymmetry in

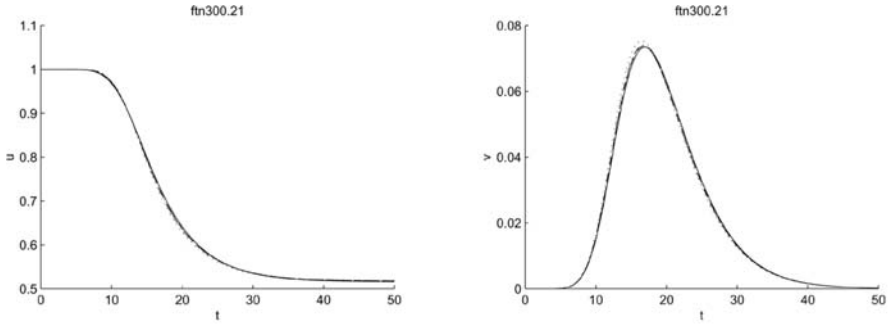

Notes: Left solid line = case 1; dashed line = case 12; dashed-dotted line = case 13; dotted line = case 14

Figure 9.
Time histories of u (left) and v (right) at $(x, y) = (1.60, 1.60)$ for boundary conditions of type 1

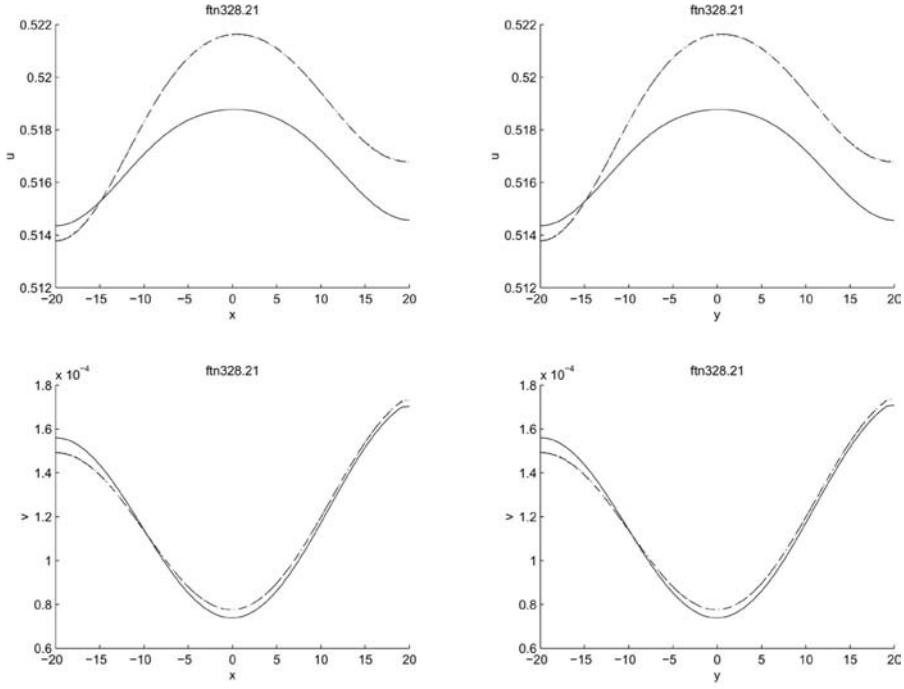

Notes: Left: solid line = case 1; dashed line = case 12; dashed-dotted line = case 13; dotted line = case 14

Figure 10.
$u(x, 0, 50)$ and $v(x, 0, 50)$ (left) and $u(0, y, 50)$ and $v(0, y, 50)$ (right) for boundary conditions of type 1

the u profiles as for cases 13 and 14 is observed in case 12. For both cases 13 and 14 of Table I, the principal directions of $\mathbf{d}$ are $(1, 1)^T$ and $(1, -1)^T$, whereas its eigenvalues are 1.1 and 0.9, and 1.5 and 0.5, respectively. Therefore, the magnitude of the Soret effects is much more important along $(1, 1)^T$ than along $(1, -1)^T$ as indicated in the u and v profiles shown in Figure 10 which clearly indicate that the values of u and v at the boundaries located at $x = L_x$ and $y = L_y$ are larger than those at $x = -L_x$ and $y = -L_y$.

The results shown in Figures 9 and 10 also indicate that, even though the time histories at (9.60, 9.60) are very similar for cases 1, 12, 13 and 14, and therefore, the arrival times of the reaction front at this location are similar, the profiles of u and v may be quite different. Therefore, one should be extremely careful when curing thermoplastics on deriving conclusions based on the arrival times of the reaction/polymerization front without accounting for the homogeneity and anisotropy of the species and temperature.

Although not shown here, it has been observed that the effects of heat diffusion on species mass diffusion (Soret effect), i.e. $\mathbf{d} \neq 0$, on the time histories of u and v are small, whereas those associated with the anisotropy of $\mathbf{k}$ are large at the location (1.60, 1.60). In fact, the time history of u at (1.60, 1.60) decreases in almost exponential manner from its initial value of 1, whereas v first increases rapidly and then decreases.

4.5 The Dufour effect

A comparison between the results presented in Figures 9 and 11 and Figures 10 and 12 indicates that the Dufour effect is more important than the Soret one for the reaction mechanism considered in this paper. In fact, case 1 predicts a faster propagating front and a larger maximum value of u at (9.60, 9.60) than cases 15-19; cases 15 and 16 result in a slighly faster reacting front than case 17. The differences between cases 15 and 16 and cases 18 and 19 are small, and these cases result in a maximum value of v smaller than that of case 1, but larger than that corresponding to case 17. However, the u and v profiles along the x and y axes shown in Figure 12 clearly indicate that the Dufour effects on the symmetry of these profiles may be important. For example, cases 18 and 19 result in almost symmetric profiles which are nearly identical to those of case 1. Case 15 also results in almost symmetric profiles, but it has steeper and thinner u and v profiles than case 1, whereas cases 16 and 17 result in clearly non-symmetric profiles characterized by relative minima at the boundaries of the domain, a relative minimum near the middle of the domain and two relative maxima. By way of contrast, the v profiles corresponding to cases 16 and 17 decrease from the bottom and left boundaries to a minimum value on the upper right quadrants and then increase monotonically as the top and right boundaries of the domain are approached. These two cases also result in values of u at the boundaries located at $x = L_x$ and $y = L_y$ which are smaller than those at $x = -L_x$ and $y = -L_y$, whereas the v profiles exhibit opposite trends, i.e., v is larger at $x = L_x$ and $y = L_y$ than at $x = -L_x$ and $y = -L_y$.

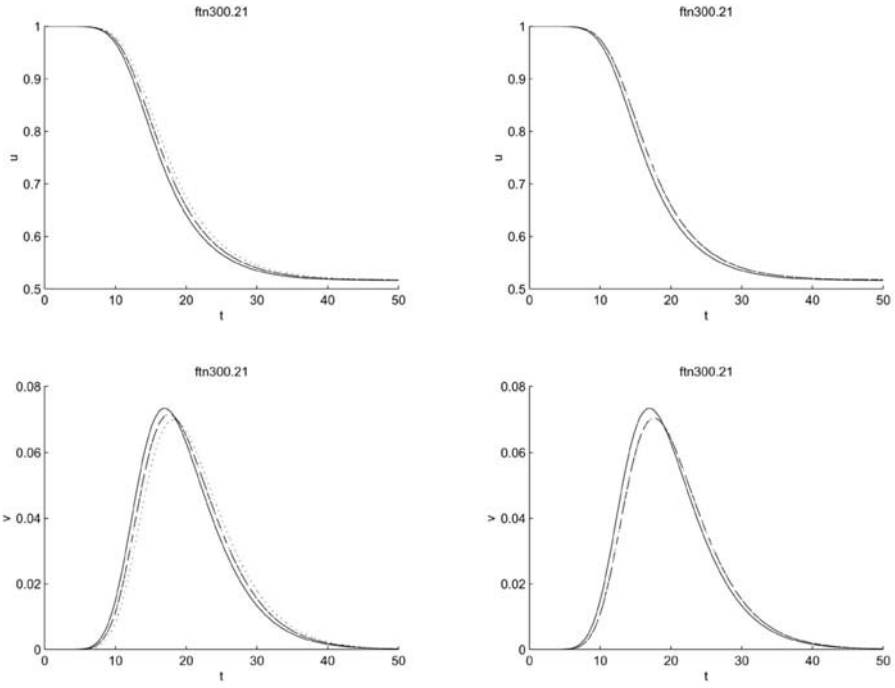

Notes: Left: solid line = case 1; dashed line = case 15; dashed-dotted line = case 16; dotted line = case 17. Right: solid line = case 1; dashed line = case 18; dashed-dotted line = case 19

Figure 11.
Time histories of u (top) and v (bottom) at $(x, y) = (9.60, 9.60)$ for boundary conditions of type 1

The asymmetries in the u and v profiles observed in Figure 12 can be explained in terms of the anisotropy of **K**. For example, case 17 corresponds to an isotropic Dufour effect in the absence of Soret effects and with isotropic heat and species diffusivity tensors, and the diffusion terms in equation (2) are enhanced by the presence of cross-diffusion where u is convex, but they are diminished where u is concave. This implies that heat diffusion enhancement occurs between the location of the propagating front and the middle of the domain.

Although, cases 15, 16, 18 and 19 correspond to anisotropic Dufour effects, and the cross-diffusion tensor corresponding to cases 15 and 16 can be diagonalized by means of a similarity transformation, it must be pointed out that, in these two cases the diffusion terms in the v-equation are enhanced due to the presence of second-order spatial derivative of u with respect to x. On the other hand, **K** cannot be diagonalized in cases 18 and 19, and the diffusion terms in the v-equation are enhanced due to the presence of second-order spatial derivative of u with respect to x and y; this enhancement caused by a mixed second-order derivative is the reason for the asymmetry of the u and v profiles exhibited in Figure 12 for cases 18 and 19.

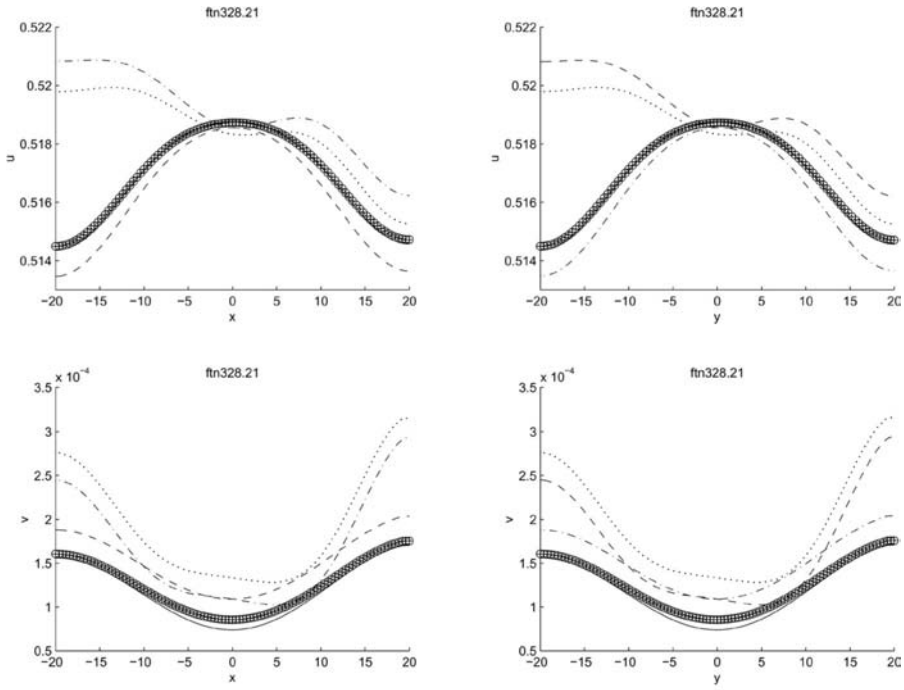

Figure 12.
$u(x, 0, 50)$ and $v(x, 0, 50)$ (left) and $u(0, y, 50)$ and $v(0, y, 50)$ (right) for boundary conditions of type 1

Notes: Left: solid line = case 1; dashed line = case 15; dashed-dotted line = case 16; cross = case 18; circle = case 19

4.6 Combined cross-diffusion effects

When there are Soret and Dufour effects and the heat and the species diffusivity tensors are isotropic, the results presented in the time histories of Figure 13 indicate that the combined cross-diffusion result in slower reaction fronts than the isotropic case 1, and the Soret and Dufour effects are much more important than either the Soret or the Dufour ones (cf. compare Figures 9 and 11 with Figure 13). In addition, case 21 results in a maximum value of v nearly identical to that of case 1, but larger than that of case 20.

Figure 14 indicates that the combined Soret-Dufour effects of cases 20-23 play an important role in determining the symmetry of the u and v profiles along the x and y axes. Thus, case 22 yields the less symmetric profiles as a consequence of the anisotropy of $\mathbf{K}$, whereas the anisotropy of $\mathbf{K}$ is of little importance as the results for cases 20, 21 and 23 indicate. These results are in accord with the Soret and Dufour effects studied on an individual bases in previous subsections, and can be explained again in terms of the eigenvalues and the principal directions of the cross-diffusion tensor $\mathbf{d}$ as follows. In case 20, $\mathbf{d}$ is isotropic, whereas, in case 21, the eigenvalues and eigenvectors of $\mathbf{d}$ are 1.5 and 0.5, and $(1, 1)^{\mathrm{T}}$ and $(1, -1)^{\mathrm{T}}$, respectively. Therefore, the cross-diffusion

effects on u are expected to be larger along the direction $(1, 1)^{T}$ than along $(1, -1)^{T}$, in agreement with the results shown in Figure 14.

Figure 14 also shows that cases 22 and 23 exhibit two relative maxima and one relative minimum in the computational domain, whereas cases 20 and 21 only exhibit a relative minimum in the computational domain.

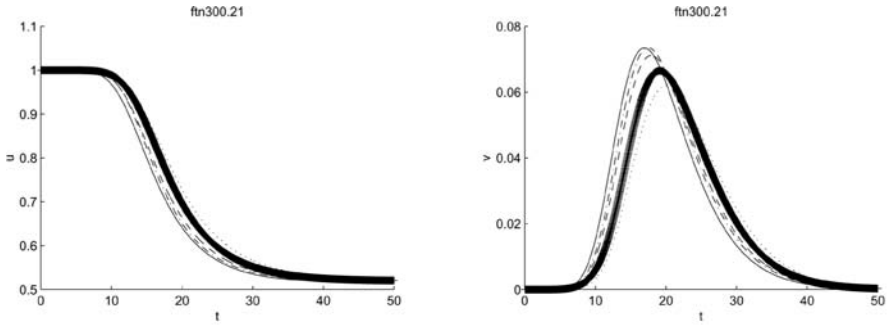

Notes: Left solid line = case 1; dashed line = case 20; dashed-dotted line = case 21; dotted line = case 22; cross = case 23

Figure 13.
Time histories of u (top) and v (bottom) at $(x, y) = (9.60, 9.60)$ for boundary conditions of type 1

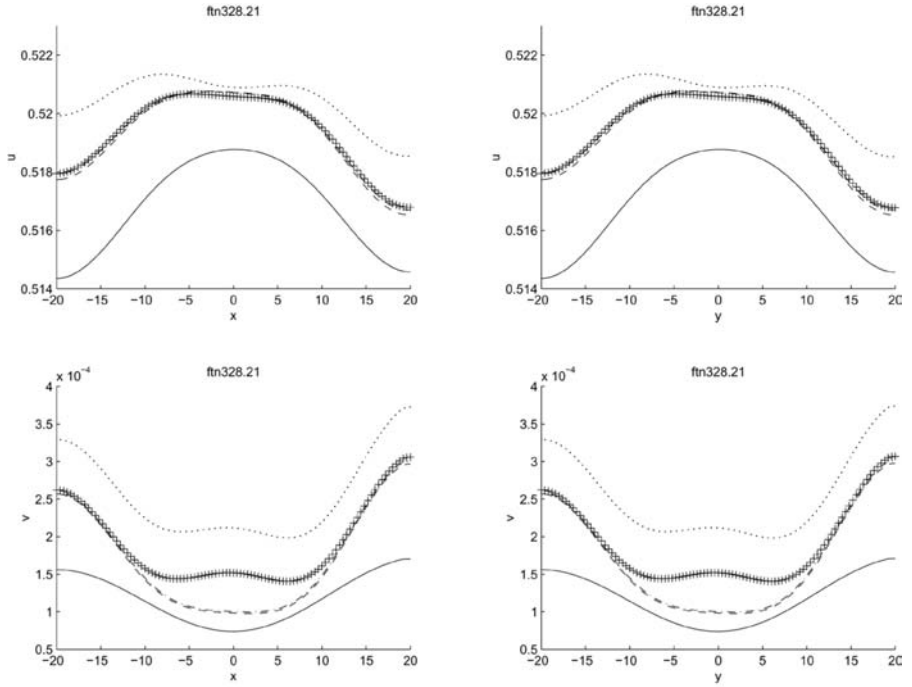

Notes: Left: solid line = case 1; dashed line = case 20; dashed-dotted line = case 21; dotted line = case 22; cross = case 23

Figure 14.
$u(x, 0, 50)$ and $v(x, 0, 50)$ (left) and $u(0, y, 50)$ and $v(0, y, 50)$ (right) for boundary conditions of type 1

4.7 Combined effects

When there are Soret and Dufour effects and either the heat or the species diffusivity tensors are anisotropic, one can find a variety of phenomena such as those shown in Figures 15 and 16. Figure 15 shows that case 28 results in a faster propagating front than case 1, which in turn predicts a faster front than

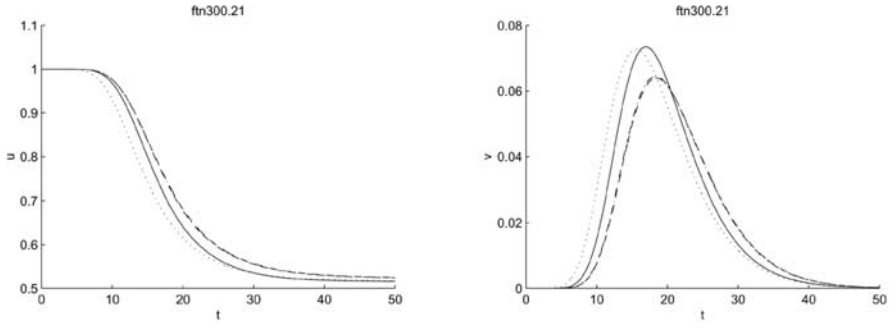

Notes: Left: solid line = case 1; dashed line = case 24; dashed-dotted line = case 25; dotted line = case 28

Figure 15.
Time histories of u (top) and v (bottom) at $(x, y) = (9.60, 9.60)$ for boundary conditions of type 1

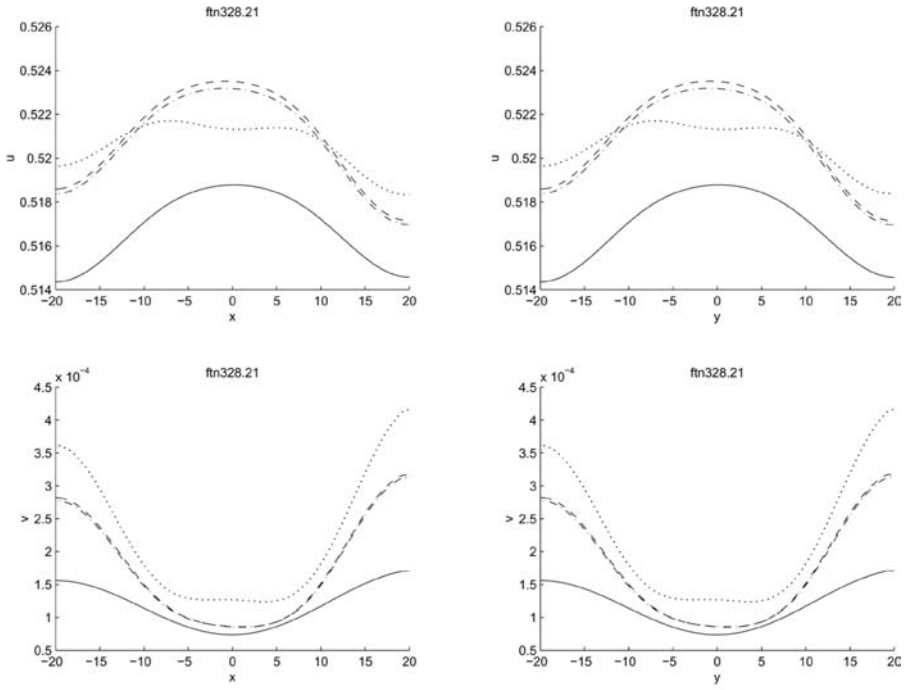

Notes: Left: solid line = case 1; dashed line = case 24; dashed-dotted line = case 25; dotted line = case 28

Figure 16.
$u(x, 0, 50)$ and $v(x, 0, 50)$ (left) and $u(0, y, 50)$ and $v(0, y, 50)$ (right) for boundary conditions of type 1

cases 24 and 25. Moreover, there are very few differences in the time histories of u and v between cases 24 and 25. In addition, case 28 predicts a slightly smaller peak value of v than the isotropic case.

A comparison between the time histories depicted in Figure 15 indicates that the anisotropy of **d** does not play an important role in the two-dimensional reactive-diffusive media with isotropic heat and species diffusion, and the anisotropy of **K** has a larger effect on the reaction front arrival time at (9.60, 9.60) than the anisotropy of **d**, in accordance with the results on the Soret effect discussed in previous subsections.

The results shown in Figure 16 indicate that case 28 results in a higher asymmetry of the u and v profiles at $t = 50$ than the isotropic case 1 and cases 24 and 25. However, cases 24 and 25 predict larger maximum values of u at (0, 0) than cases 1 and 28, and cases 1, 24 and 25 exhibit a relative maximum of u and a broad valley of v in the computational domain, whereas case 28 predicts two relative maxima and a relative minimum in both u and v in the domain.

The results shown in Figure 16 can once again be explained in terms of the principal directions of the diffusivity tensors **k**, **d**, **K** and **D**, and indicate that the values of u and v at $x = L_x$ and $y = L_y$ are smaller and larger, respectively, than those at $x = -L_x$ and $y = -L_y$, i.e. the values of u and v along $(1, 1)^{\mathrm{T}}$ are smaller and larger, respectively, than along $(1, -1)^{\mathrm{T}}$.

The results depicted in Figures 5-16 are of paramount importance to determine the reaction-diffusion processes in the anisotropic media, combustion of solid materials, heat and mass transfer in anisotropic media, the time and homogeneity of the curing of thermosetting matrix composites, the laser-grooving of fibre-reinforced orthotropic composite materials, and the laser-induced thermal damage of fibres, for they show the arrival of the reaction fronts as well as the histories of the species mass fractions and temperature, as functions of the anisotropy of the species and heat diffusivities and the Soret and Dufour effects. These figures indicate that the arrival time at a monitor location is not an adequate measure of the uniformity of the species and heat profiles in, say, the curing of thermosetting matrix composites. In addition, these figures indicate that the time required to achieve a steady solution which must be homogeneous because of the homogeneous Neumann boundary conditions employed in this paper is a strong function of the anisotropy of the heat and species diffusivity tensors and the Soret and Dufour effects. In fact, the time required to reach a steady state solution increases as the anisotropy of the heat and species diffusivity tensors increases, when there are no Soret and Dufour effects; it is nearly independent of the Soret effect for isotropic heat and species diffusivities in the absence of the Dufour effect, decreases with the presence of Dufour effects in the absence of Soret ones, and decreases in the presence of Soret and Dufour effects as the anisotropy of either the heat or the species diffusivity tensor is increased.

4.8 Effects of the boundary conditions

So far, we have restricted our discussion of results to those corresponding to boundary conditions of type 1, which are much easier to implement numerically than, for example, boundary conditions of type 5.

For the cases considered in this paper, it has been found that there are very few differences between the results obtained with boundary conditions of types 1-5, except in cases 6 and 23 along the axes $x = 0$ and $y = 0$. Some sample results that illustrate the differences in the u and v profiles obtained with the five boundary conditions employed in this paper are shown in Figures 17-19 which correspond to cases 12, 6 and 23, respectively, and show $u(0, y, t)$ and $v(0, y, t)$ at $t = 32$ (top) and $u(x, 0, t)$ and $u(x, 0, t)$ at $t = 50$ (bottom). The solid lines in these figures correspond to the boundary conditions of type 1 which produce nearly identical results to the boundary conditions of types 2 and 3, whereas the boundary conditions of type 4 yield nearly identical results to the boundary conditions of type 5.

The results depicted in Figure 17 indicate that the differences in the u and v profiles along the x and y axes for the five boundary conditions employed in

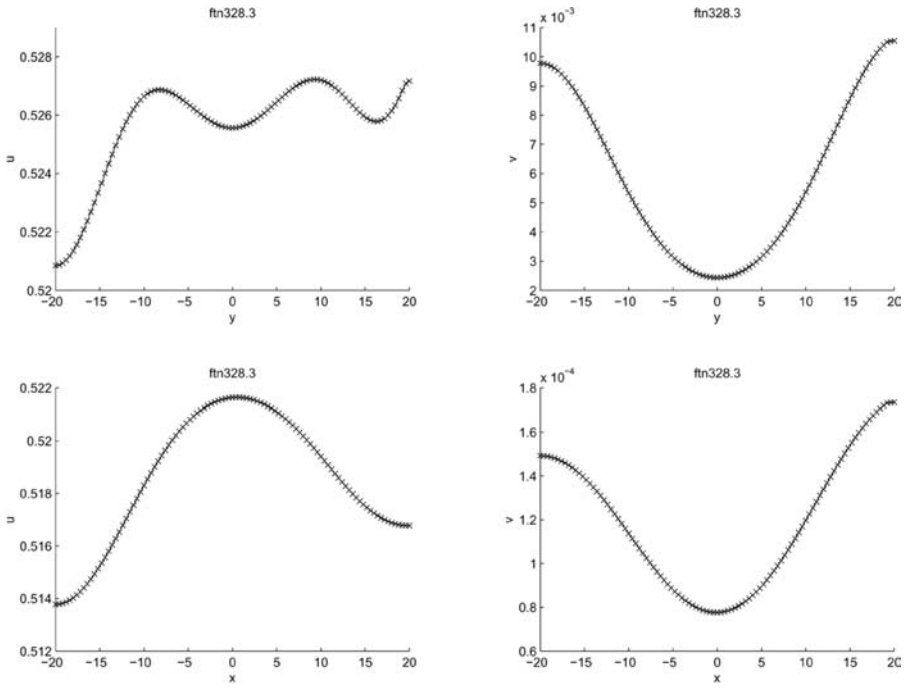

Notes: Solid line = boundary conditions of type 1; dashed line = boundary conditions of type 2; dashed-dotted line = boundary conditions of type 3; dotted line = boundary conditions of type 4; cross = boundary conditions of type 5

Figure 17.
$u(0, y, 32)$ (top left), $v(0, y, 32)$ (top right), $u(x, 0, 50)$ (bottom left) and $v(x, 0, 50)$ (bottom right) for case 12

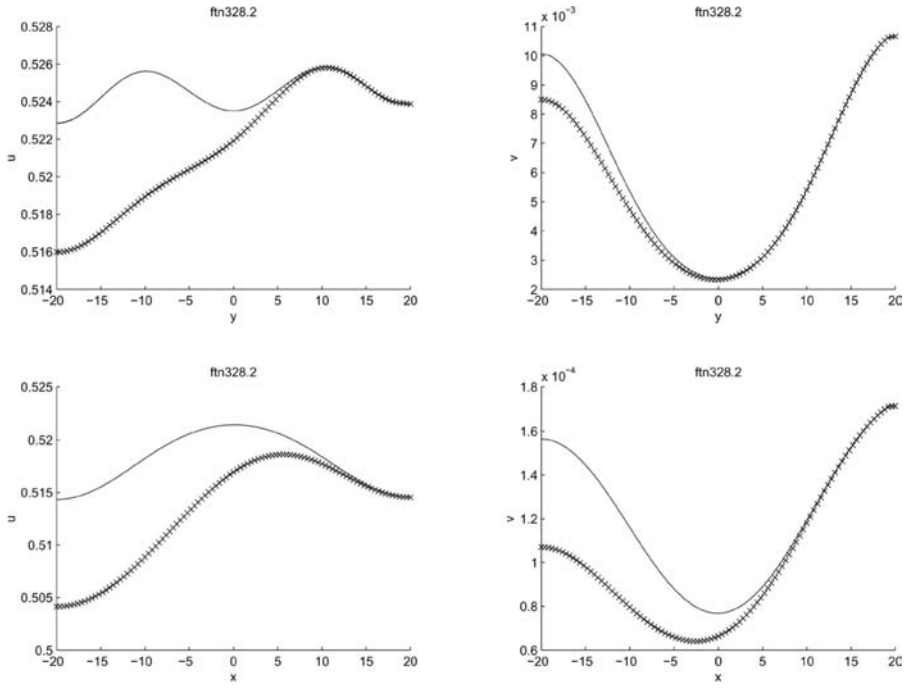

Notes: Solid line = boundary conditions of type 1; dashed line = boundary conditions of type 2; dashed-dotted line = boundary conditions of type 3; dotted line = boundary conditions of type 4; cross = boundary conditions of type 5

Figure 18.
$u(0, y, 32)$ (top left), $v(0, y, 32)$ (top right), $u(x, 0, 50)$ (bottom left) and $v(x, 0, 50)$ (bottom right) for case 6

this study is rather small for case 12 at $t = 32$ and 50. Very small differences in u and v have also been observed along the boundaries. However, the results for case 6 exhibited in Figure 18 clearly indicate that even though the differences between the boundary conditions of types 1, 2 and 3 are small, the differences between the results corresponding to these conditions and those of boundary conditions 4 and 5 are large near the boundaries located at $x = -L_x$ and $y = -L_y$ in accordance with the discussion of the eigenvectors and eigenvalues of $\mathbf{k}$ presented in previous sections.

For case 23 of Table I, the results depicted in Figure 19 show that the boundary conditions of types 1-3 produce nearly identical results, and these results have similar shapes to those boundary conditions 4 and 5 at $t = 32$. At $t = 50$, boundary conditions of types 1-3 predict larger values of u at the left boundary than boundary conditions 4 and 5 in this order, while the steepest u velocity profile at this time is associated with the boundary conditions of type 5.

Calculations performed until a steady state was achieved show that the five types of boundary conditions used in this paper predict the same (steady)

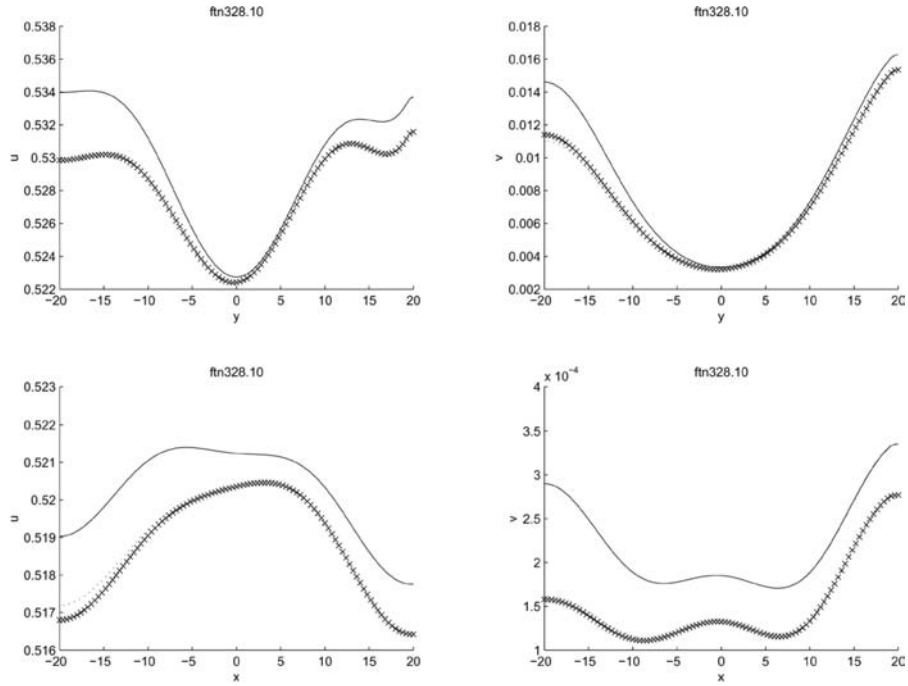

Figure 19.
$u(0, y, 32)$ (top left), $v(0, y, 32)$ (top right), $u(x, 0, 50)$ (bottom left) and $v(x, 0, 50)$ (bottom right) for case 23

Notes: Solid line = boundary conditions of type 1; dashed line = boundary conditions of type 2; dashed-dotted line = boundary conditions of type 3; dotted line = boundary conditions of type 4; cross = boundary conditions of type 5

values of u and v, the time required to achieve this state depends on the type of boundary conditions employed, and boundary conditions of type 5 required longer times to achieve steady state.

5. Conclusions

Non-linear reactive-diffusive phenomena in two-dimensional, anisotropic media with cross-diffusion have been studied numerically by means of an implicit, iterative, time-linearization, approximate factorization technique as functions of the anisotropy of the heat and species diffusivity tensors and cross-diffusion for five types of boundary conditions. It has been shown that the anisotropy of the diffusivity tensors induces deformations of the front and affects the front velocity. The magnitude of these effects increases as the magnitude of the off-diagonal components of the heat and species diffusivity tensors is increased. For the cases considered in this paper, it has been found that cross-diffusion effects, i.e. the Soret and Dufour effects, affect less the reaction front shape and velocity than the anisotropy of the heat and species diffusivity tensors.

It has also been found that the five types of boundary conditions employed in this study produce similar results except when there is either strong anisotropy in the species or heat diffusivity tensors and there are no Soret and Dufour effects, or the species and heat diffusivity tensors are isotropic but the Soret and Dufour effects are anisotropic and important. If the species and heat diffusivity tensors are isotropic, the effects of either Soret or Dufour cross-diffusion are small for the cases considered in this study.

It has also been found that the time required to achieve steady state conditions in two-dimensional, anisotropic, reactive-diffusive media increases as the anisotropy of the heat and species diffusivity tensors increases when there are no Soret and Dufour effects, is nearly independent of the Soret effect for isotropic heat and species diffusivities in the absence of the Dufour effect, decreases as the magnitude of the Dufour effect is increased in the absence of Soret ones, and decreases in the presence of Soret and Dufour effects as the anisotropy of either the heat or the species diffusivity tensor is increased. Therefore, the time required to achieve homogeneity in the curing of thermosetting matrix composites increases as the anisotropy of the heat and species diffusivity tensors increases. It has also found that the boundary conditions of type 5 required longer times to achieve steady state than the other four types of boundary conditions considered here, the differences between the boundary conditions of types 1-3 are small, and boundary conditions of type 4 produced nearly identical results to boundary conditions of type 5.

References

Beam, R.M. and Warming, R.F. (1978), "An implicit factored scheme for the compressible Navier-Stokes equations", *AIAA J.*, Vol. 16, pp. 393-402.

Benano-Melly, L.P., Caltagirone, J-P., Faissat, B., Montel, F. and Costeseque, P. (2001), "Modeling Soret coefficient measurement experiments in porous media considering thermal and solutal convection", *Int. J. Heat Mass Transfer*, Vol. 44, pp. 1285-97.

Briley, W.R. and McDonald, H. (1980), "On the structure and use of linearized block implicit methods", *J. Comput. Phys.*, Vol. 34, pp. 54-73.

Briley, W.R. and McDonald, H. (2001), "An overview and generalization of implicit Navier-Stokes algorithms and approximate factorization", *Computers and Fluids*, Vol. 30, pp. 807-28.

Hsieh, M-H. and Ma, C-C. (2002), "Analytical investigations for heat conduction problems in anisotropic thin-layer media with embedded heat sources", *Int. J. Heat Mass Transfer*, Vol. 45, pp. 4117-32.

Kowsary, F. and Arabi, M. (1999), "Monte Carlo solution of anisotropic heat conduction", *Int. Comm. Heat Mass Transfer*, Vol. 26, pp. 1163-73.

MacCormack, R.W. (2001), "Iterative modified approximate factorization", *Computers and Fluids*, Vol. 30, pp. 917-25.

Mera, N.S., Elliott, L., Ingham, D.B. and Lesnic, D. (2001), "A comparison of boundary element method formulations for steady state anisotropic heat conduction problems", *Engineering Analysis with Boundary Elements*, Vol. 25, pp. 115-28.

Ramos, J.I. (1999), "Linearized factorization techniques for multidimensional reaction-diffusion equations", *Appl. Math. Comput.*, Vol. 100, pp. 201-22.

Skarda, J.R.L., Jacqmin, D. and McCaughan, F.E. (1998), "Exact and approximate solutions to the double-diffusive Marangoni-Bénard problem with cross-diffusive terms", *J. Fluid Mechanics*, Vol. 366, pp. 109-33.

Steinthorsson, E., Li, Z., Shih, T.I-P., Nguyen, H.L. and Willis, E.A. (1991), "Flux-vector splitting algorithm for chain-rule conservation-law form", *AIAA J.*, Vol. 29, pp. 1101-7.

Traiano, F.M.L., Cotta, R.M. and Orlande, H.R.B. (1997), "Improved approximate formulations for anisotropic heat conduction", *Int. Comm. Heat Mass Transfer*, Vol. 24, pp. 869-78.

Williams, F. (1985), *Combustion Theory*, 2nd ed., Addison-Wesley Publishing Company, New York.

Yi, S., Hilton, H.H. and Ahmad, M.F.D. (1997), "A finite element approach for cure simulation of thermosetting matrix composites", *Computers and Structures*, Vol. 64, pp. 383-8.